Engineering Structures 293 (2023) 116713

Contents lists available at ScienceDirect

Engineering Structures

journal homepage: www.elsevier.com/locate/engstruct

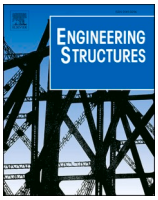

Parametric investigation on the response of suspended piping systems to tri-directional seismic excitation

Gianni Blasi *, Daniele Perrone, Maria Antonietta Aiello

Department of Engineering for Innovation, University of Salento, Italy

ARTICLE INFO

Keywords:
Piping systems
Vertical acceleration
Seismic vulnerability
Parametric analysis
Numerical modelling
Non-linear dynamic analysis

ABSTRACT

The evaluation of the seismic performance of piping networks is often difficult due to several parameters involved in the process, such as complex geometry, modelling uncertainties and earthquake properties. Despite several studies have been conducted on this topic, driven by the importance of piping networks from a building serviceability standpoint, generalized guidelines to achieve defined performance criteria are still difficult to develop. The hardships in analysing the seismic response of piping networks are mainly due to their peculiar configuration, which leads to interaction between local vibration modes and the seismic acceleration. Additional issues are also caused by great variability in piping systems' design and quality. The scope of this study is to investigate several aspects of the dynamic response of different types of piping networks, considering tri-directional floor seismic input. A numerical model was developed, accounting for the non-linear behaviour of piping restraint installations and pipe joints. The numerical model was used to perform nonlinear time-history analyses aimed at assessing the seismic vulnerability in a performance-based design framework. The influence of the geometric configuration and the mass of the system was investigated by analysing the accelerations and displacements, alongside damage on pipe joints and suspended piping restraints due to earthquake. Additionally, the response obtained considering and neglecting the vertical component of the floor acceleration were compared. The results of the analysis were employed to compute fragility functions at different limit states, considering the parameters investigated. A clear influence of the geometry and the mass of the system on the seismic vulnerability is observed, while the effects of the vertical acceleration seem to be generally negligible.

1. Introduction

The increasing attention paid by modern design codes on the seismic performance of non-structural components (NSCs) [1–3] testifies the importance of this issue in performance-based earthquake engineering (PBEE) frameworks. In fact, post-earthquake damage surveys highlighted the vulnerability of NSCs and their importance from an economic loss standpoint [4–7]. This issue was also evidenced by a number of numerical studies focused on the earthquake loss estimation and risk assessment [8]. In most of the codes and guidelines, the seismic design/assessment of NSCs in encouraged by providing simplified models to compute seismic demand, depending on the ductility capacity, the dynamic properties and the importance of the considered component. However, several parameters may influence the dynamic response of NSCs, leading to hardships in adopting simplified formulations. In order to overcome the shortcomings of the code provisions in predicting the non-structural seismic demand, recent studies proposed more accurate procedures accounting for several additional parameters [9–11]. The "cascade methods" are advanced approaches widely adopted in non-structural analysis and consist in generating the seismic demand on NSCs based on the analysis of the structural system.

In some cases, NSCs have high importance in both serviceability of a building and life-safety [4,6] and the accurate definition of their seismic performance is fundamental. To this regard, piping systems are emblematic, since their operation may be required also in the immediate post-seismic emergency (e.g. fire-fighting or medical gas distribution systems). For this reason, several research studies were addressed at characterizing the seismic vulnerability of such NSCs. Advanced analyses were conducted on single pipe lines with composite materials, to investigate the effect of manufacturing-induced uncertainties on non-linear dynamic response [12]. Several studies were also carried out on buried pipelines with simple layout, to analyse local failure when subjected to transverse loading [13,14].

However, the complex layout of suspended piping systems installed

* Corresponding author.
E-mail address: gianni.blasi@unisalento.it (G. Blasi).

https://doi.org/10.1016/j.engstruct.2023.116713
Received 8 February 2023; Received in revised form 28 April 2023; Accepted 30 July 2023
Available online 4 August 2023

in civil buildings requires a global approach when analysing their seismic response. In fact, the highly different boundary conditions compared to buried pipes have major influence on global dynamics. Recent works focused on fire-protection piping systems in strategic and public buildings. Laboratory tests and numerical analyses were conducted to assess the dynamic behaviour of different piping system configurations [15,16] showing failure of pipe joints and piping restraints when subjected to seismic action. Numerical simulations were performed in last years to identify reliable seismic design methods for piping systems, by comparing fragility functions depending on the design approach adopted [17,18].

The outcome of the recent research showed major hardships in defining the seismic vulnerability of piping systems, mainly related to the peculiar configurations of the networks, as well as their high irregularity. Despite the great efforts made in characterizing the non-linear response of single components by laboratory testing, such as piping restraining elements [19,20] or pipe joints [21–23], the definition of simplified models for global analysis is still challenging. In fact, the dynamic properties of piping systems are influenced by a large number of aspects, such as type and location of piping restraints and connections between pipes, presence of vertical and horizontal necks, and so on. In some cases, only simple rods or cables are employed to connect the pipes to the structures, which may lead to several effects from a seismic performance standpoint. For instance, the absence of braced restraints causes high displacements in case of earthquake, leading to possible damage due to impact between pipes. Additionally, gravity restraints may act as tie elements, leading to high sensitivity to vertical accelerations. It is simply to understand that these aspects are significantly connected to specific architectural requirements, which are significantly variable.

In this study, the seismic vulnerability of fire-fighting and medical gas distribution piping systems is analysed, by mean of non-linear dynamic analysis. A simple geometry is considered for the networks analysed, composed of a main line and two branch lines. The piping systems are modelled using OpenSees [24], simulating the non-linear hysteretic response of piping restraints and pipe joints to detect damage due to earthquake. Different layouts configurations were considered, varying the location of the branch lines and the number of pipes in the main line, to analyse their influence on damage of pipe joints and piping restraints in the presence of seismic action. Numerical dynamic analyses were conducted, using, as input motion for the piping systems, floor acceleration time-histories generated from the analysis of a case study infilled RC frame examined in a previous work [18]. The influence of the vertical acceleration on the seismic fragility of the case study piping systems was also assessed. For each piping layout considered, non-linear time-history analyses were conducted either assuming and neglecting the vertical acceleration, comparing the damage to pipe joints and piping restraints. Lastly, fragility functions were computed for all the analysed configurations, aiming to evaluate the influence of the considered parameters on the seismic performances.

2. Description of the case study piping systems

The medical gas distribution and fire protection piping systems (MP and FP, respectively) analysed in this study were assumed to be installed in an 8-storey healthcare facility. The network of both MP and FP, characterized by copper and steel pipes, respectively, was composed of a main line and two branch lines (Fig. 1). The piping systems were directly connected to the slab of the building, through gravity and seismic piping restraint installations, characterized by simple cables and trapezes with longitudinal and transverse braces, respectively (Fig. 2). The height of all restraints was equal to 600 mm, while the length of horizontal channels in restraints for multiple pipes (Fig. 2**c** and **d**) was equal to 900 mm. 45° braces with length equal to 850 mm were assumed for seismic restraints. Referring to FP, the main line and the branch lines were composed of 60.3 mm (2″) and 33.7 mm (1″) steel pipes, respectively, with threaded pipe joints. The dimension of the pipes was defined depending on the required water flow prescribed in [25]. In case of MP,

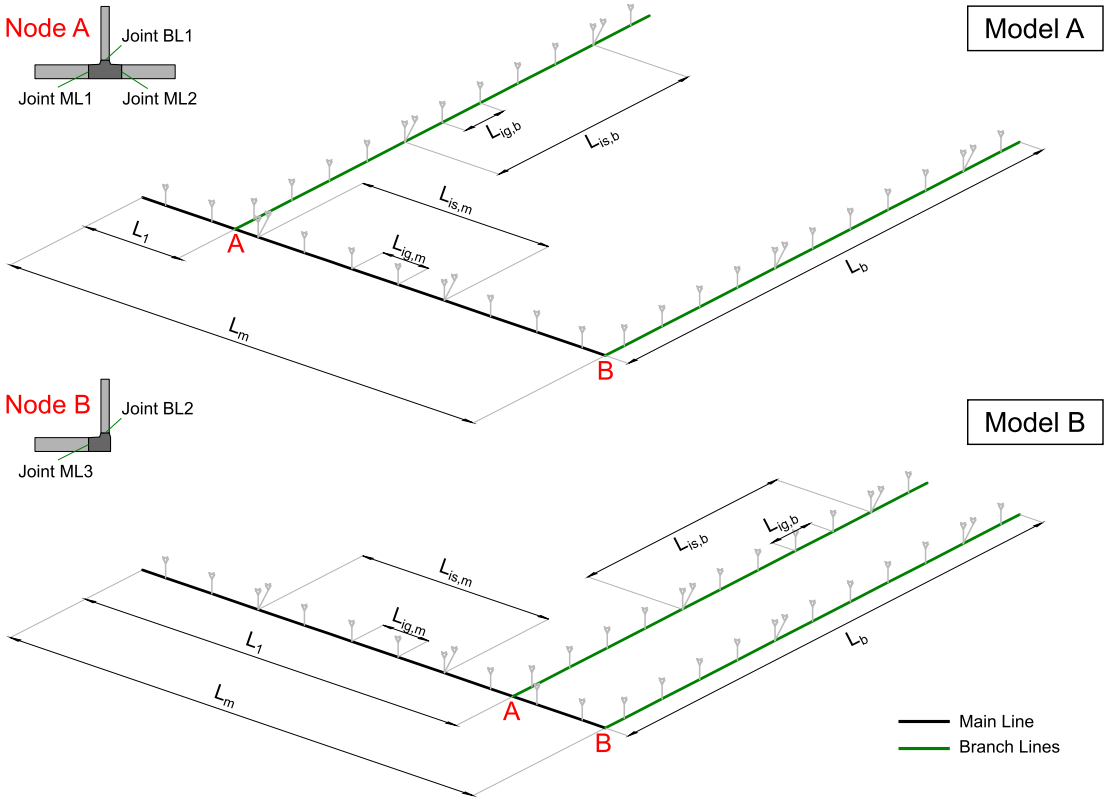

Fig. 1. Geometry of MP and FP networks.

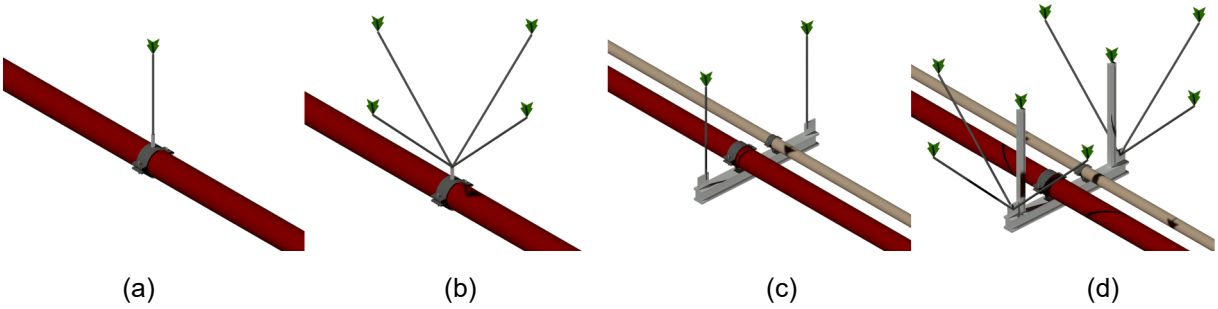

Fig. 2. Illustration of suspended piping restraints adopted for the analysed systems: (a) single cables in branch lines, (b) braced restraint in branch lines (c) double cable in main line and (d) braced restraint in main line.

the main and the branch lines were composed of 54.0 mm and 28.0 mm pipes, with welded pipe joints, according to [26]. Aiming to assess the influence of the geometry of the network on the seismic response of the piping systems, two layouts were considered for each configuration. The two layouts (Model A and Model B, respectively in Fig. 1) differ from the distance of the first branch line from the first node of the main line (L_1 in Fig. 1).

In the main line, each restraint hosted both MP and FP pipes, alongside additional pipe lines, as shown in Fig. 2**c** and **d**. This assumption is consistent with the configurations usually observed in strategic buildings, where main pipes of several piping networks are often arranged along the same line, to minimize the number of suspended piping restraints and ease design and maintenance. To this regard, a variation of the total mass of the system and, consequently, its dynamic response, is expected, depending on the number of pipes rigidly connected to piping restraints. Since this number is defined based on architectural and serviceability requirements, four configurations of the main line were analysed herein. In the first configuration (**C_1**), one additional steel pipe was included in the main line alongside either the copper (for MP) or the steel (FP) pipe line. In the remaining configurations, named **C_2**, **C_3** and **C_4**, either three, five, and seven water distribution steel pipes, having 114.3 mm diameter, respectively, were included in the main line alongside the MP and the FP pipes. It is worth mentioning that the branch lines were composed of one single pipe (either copper or steel in case of MP and FP, respectively).

The main properties of the piping layouts are provided in Table 1. The values of L_1 and L_m, representing the distance of the first branch line from the first node of the main line, and the length of the main line, respectively, are expressed as function of $L_{ig,m}$. This symbol represents the spacing between the gravity supports and varies depending on the number of pipes in the main line.

The spacing between suspended piping seismic restraints, referred as $L_{is,m}$ and $L_{is,b}$ for main line and branch lines, respectively (Fig. 1), was defined based on a simplified seismic design, according to Italian NTC18 [3]. Therefore, the equivalent static force, F_{Hr}, acting on the single restraint, was computed according to the formulation:

$$F_{Hr} = \frac{W_{ns} S_{ans}}{q_{ns}} \tag{1}$$

In equation (1), W_{ns} is the piping weight aliquot assigned to the single seismic restraint, evaluated as the product between the pipeline unit weight and the spacing between restraints. S_{ans} is the spectral acceleration demand of the system and q_{ns} is the behaviour factor of the element considered, assumed equal to 1.0. The adopted formulation is similar to those provided in other codes (e.g. [27,28]), although it does not account for the importance of the considered element. Moreover, a very limited classification for q_{ns} is provided in Italian code. W_{ns} was computed for each layout configuration (i.e. C_1, C_2, C_3 and C_4). Hence, different values were obtained depending on the number of pipes in the main line. The mass of the system was calculated considering the presence of water in all the pipes in main line and branch lines, except for the MP pipe.

The value of S_{ans} was computed adopting the simplified formulation (2) provided by Italian NTC18 [3]:

$$S_{ans} = PGA \bullet S_s \left\{ \frac{5 \bullet \left(1 + \frac{z}{h}\right)}{\left[1 + 4\left(1 - \frac{T_{ns1}}{0.8 \bullet T_{f1}}\right)^2\right]} \right\} \tag{2}$$

In equation (2), PGA and S_s are the peak ground acceleration and the soil coefficient, respectively, z and h are the quote of the piping system and the height of the structure, respectively, T_{ns1} and T_{f1} are the fundamental periods of the piping system and the structure, respectively. S_{ans} was calculated according to a conservative approach, assuming $T_{ns1}/T_{f1} = 1$. The results obtained from the simulated design of each configuration considered are provided in Table 2. The same value of $L_{is,m}$ was eventually adopted in case of C_1 and C_2, because a maximum seismic restraints' spacing was set. Since Italian code does not include provisions on such aspect, the maximum spacing assumed was equal to that suggested by NFPA 13 [29]. This assumption also led to the adoption of the same value of $L_{is,b}$ and, consequently, of gravity supports' spacing ($L_{ig,b}$) and total length of the branch lines (L_b) in all configurations. Lastly, the same seismic restraints spacing in MP and FP was obtained.

Table 1
Properties of the piping system layouts analysed.

ID	MP		FP	
	Main Line	Branch Line	Main Line	Branch Line
Pipe diameter [mm]	54.0	28.0	60.3	33.7
Pipe material	copper	copper	steel	steel
Pipe's Young's modulus [MPa]	113,086	113,086	194,383	194,383
L_1 model A	$2 \cdot L_{igm}$	–	$2 \cdot L_{igm}$	–
L_1 model B	$8 \cdot L_{igm}$	–	$8 \cdot L_{igm}$	–
L_m	$10 \cdot L_{igm}$	–	$10 \cdot L_{igm}$	–
L_b [m]	–	38.5	–	38.5
Joint type	welded	welded	threaded	threaded

Table 2
Details of the piping network configurations analysed.

ID	C_1	C_2	C_3	C_4
N. of pipes in main line	2	4	6	8
$L_{ig,m}$ [m]	3.50	3.50	3.25	2.50
$L_{is,m}$ [m]	10.50	10.50	6.50	5.00
$L_{ig,b}$ [m]	3.50	3.50	3.50	3.50
$L_{is,b}$ [m]	10.50	10.50	10.50	10.50

2.1. Description of the numerical model

The MP and the FP systems were modelled and analysed separately, considering in each model the additional mass due to the presence of multiple pipes in the main line, without explicitly modelling additional lines. The numerical model was developed by adopting a lumped plasticity approach in OpenSees [24]. Linear elastic beam elements were used to simulate pipes, including zero-length bi-directional flexural springs (Fig. 3) to reproduce the hysteretic moment-rotation behaviour (M-θ) at the joint between multiple pipes. The non-linear response of suspended piping seismic restraints was simulated including non-linear zero-length shear springs, oriented in both horizontal directions. Gravity piping restraints were modelled using zero-length axial springs acting in vertical direction (Fig. 3). Uneven positive and negative response in the vertical direction was set for gravity restraints, accounting for axial buckling.

The mass matrix was defined in the numerical model through a smeared approach, assigning a unit length mass to each linear beam element representing the pipe. The damping of the system was simulated adopting the Rayleigh method [30], by defining a mass-proportional damping for nodes with mass and a stiffness-proportional damping for linear elements and lumped hinges. The mass-proportional ($\alpha_{\boldsymbol{M}}$) and the stiffness-proportional ($\beta_{\boldsymbol{K}}$) damping coefficients were evaluated as function of the frequencies of the two modes with higher participating mass ratio and the damping ratio. Two different values of damping ratio were considered for FP and MP, equal to 2% and 5% respectively, according to the values obtained experimentally from Blasi et al. [23].

The non-linear response of pipe joints was simulated using the Pinching4 uniaxial material [31]. Referring to FP system, two different hysteretic models were defined for 60.3 and 33.7 pipe joints, respectively (i.e. for pipe connection in main and branch lines, respectively). The parameters defining the M-θ backbone curve and the pinching behaviour were calibrated in order to match the cyclic curves obtained from laboratory tests [23,32]. The hysteretic M-θ behaviour defined in OpenSees is provided in Fig. 4**a** and **b** for 60.3 and 33.7 pipe joints, respectively. It is worth mentioning the significant difference between the hysteretic loops obtained for the two pipe joints. This outcome could be explained by the height of the threads, which is identical in 60.3 and 33.7 mm joints [33]. Hence, in case of 60.3 pipe joints, the ratio between the threads' height and the cross-section diameter of the pipe is relatively low. Consequently, damage is mainly due to threads failure and subsequent increase of gaps between the remaining threads, significantly reducing stiffness during the load-inversion phase. On the other hand, the ratio between the threads' height and the cross-section diameter of the pipe is greater in 33.7 mm joints, leading to higher flexural strain of the cross section alongside threads damage. This damage mode leads to generation of smaller gaps between threads and less pronounced pinching effect.

Also in case of MP, the Pinching4 moment-rotation behaviour of welded pipe joints (Fig. 5) was calibrated based on the hysteretic curves obtained experimentally by Blasi et al. [23,34]. The failure mode of such tee-joints subjected to cyclic loading features local buckling of the tee element. Consequently, the pinching effect was nearly absent in this case. Additionally, it is worth mentioning the significant difference between the enveloped cyclic response and the monotonic response obtained (Fig. 5). This phenomenon is caused by the major distortion of the joint's geometry caused by local buckling, which leads to second order resisting mechanisms at the load inversion.

Both gravity and seismic restraints were simulated including zero-length non-linear springs, acting in vertical and in the two horizontal directions, respectively, and directly connected to the elements simulating the pipes. The mechanical behaviour of gravity supports was defined assuming a tri-linear elastic-hardening–softening axial force–deformation (F-d) response in tension only (Fig. 6**a**). A classical approach was adopted to calibrate the yielding and ultimate point in the F-d bi-linear curve, based on the cross-sectional area of the cables and steel's yielding and ultimate strength, respectively. The softening slope was aimed at simulating tensile failure of the cable, arbitrarily assuming residual strength and deformation values as 10% and 120% of ultimate strength and ultimate deformation, respectively. Near-zero strength and stiffness were considered in compression, since buckling load was negligible compared to yielding strength in tension.

The F-d behaviour of the lumped springs simulating seismic restraints (Fig. 6**b**) corresponds to the transverse response of the braced elements. A similar behaviour was assumed for the response of longitudinal braced elements, according to experimental findings in [35]. Similarly to pipe joints, the pinching parameters and the backbone curve points in the F-d curve were calibrated based on laboratory tests results [35].

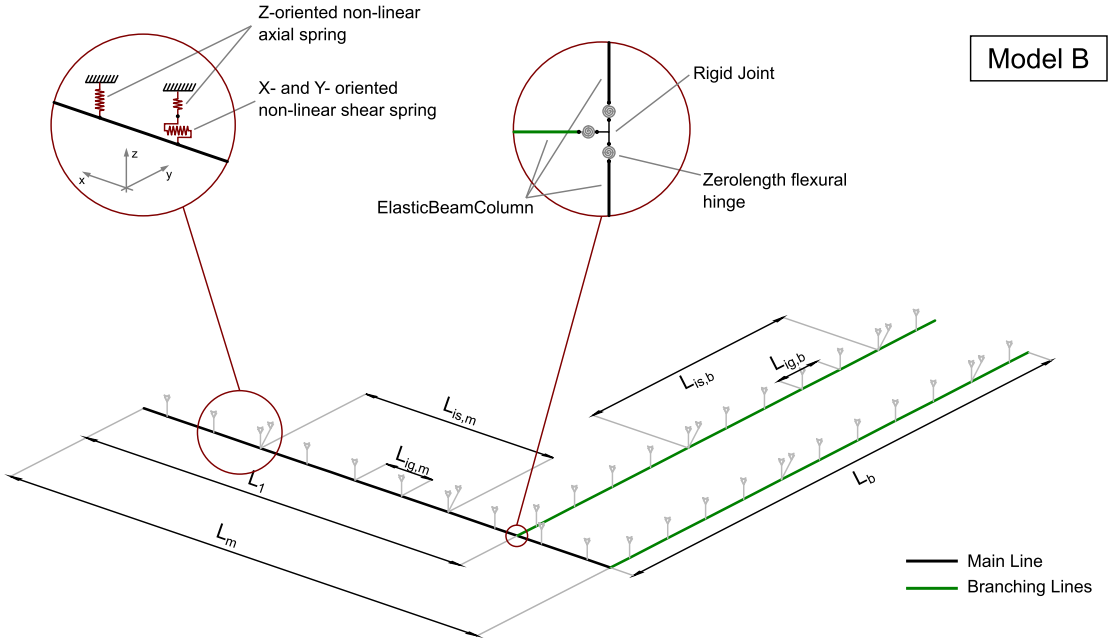

Fig. 3. Description of the modelling approach adopted in the numerical simulation.

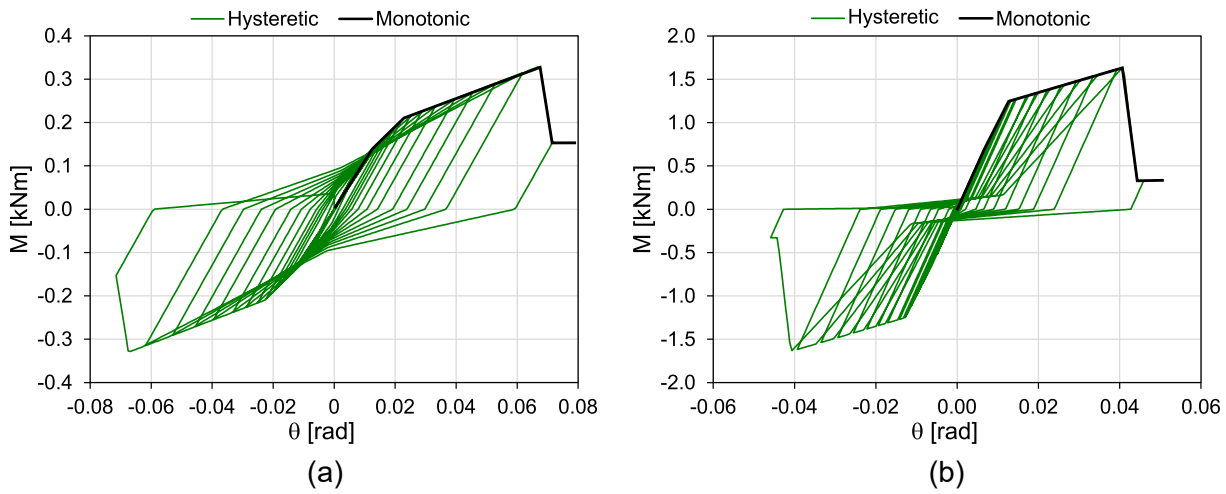

Fig. 4. Mechanical model (Pinching4 material) adopted for the simulation of the hysteretic M-θ response of (a) 33.7 mm and (b) 60.3 mm threaded steel joints.

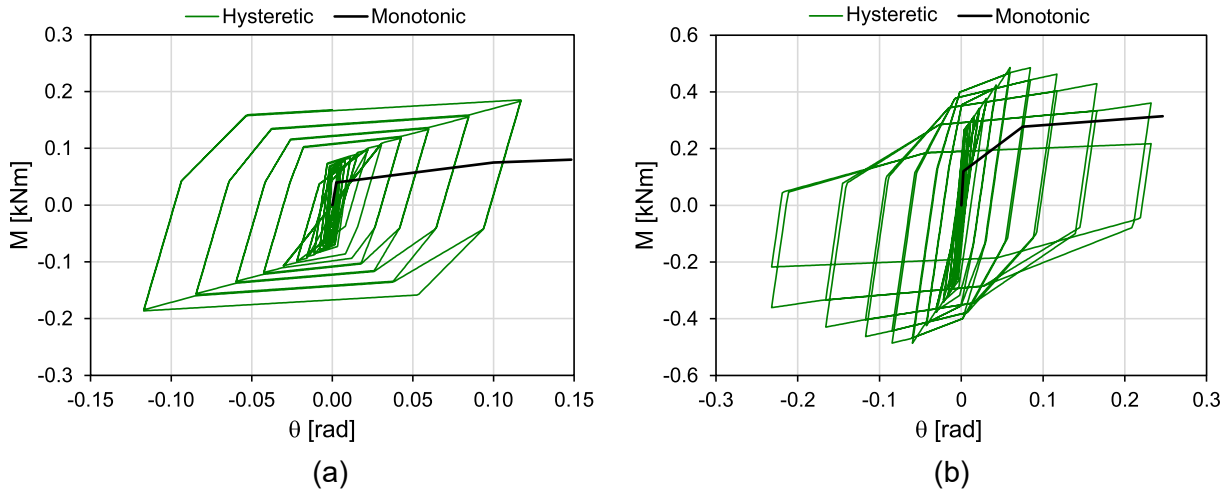

Fig. 5. Mechanical model (Pinching4 material) adopted for the simulation of the hysteretic M-θ response of (a) 28 mm and (b) 54 mm welded copper joints.

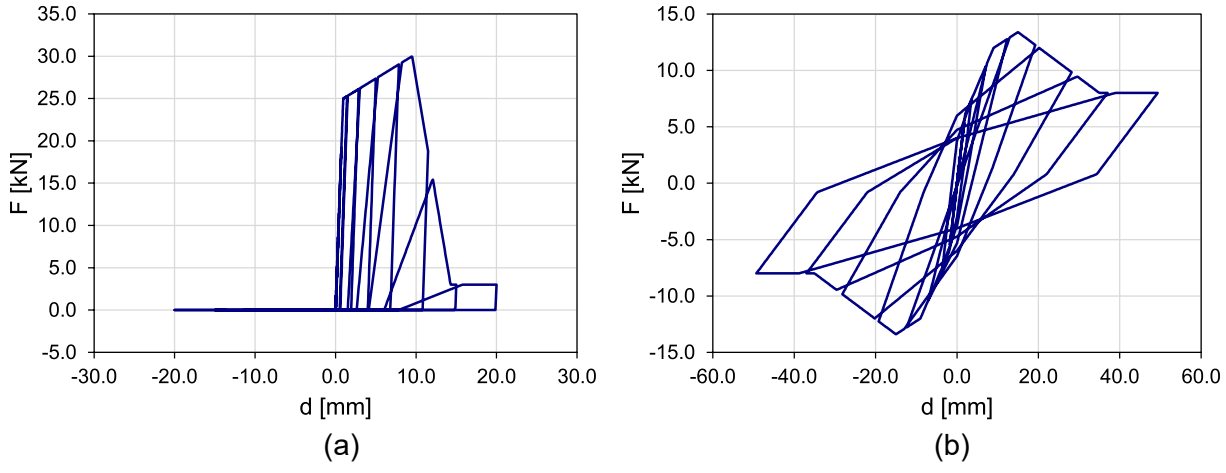

Fig. 6. Hysteretic F-d behaviour in numerical model for (a) gravity restraints and (b) seismic restraints.

3. Cascade analysis

3.1. Analysis setting

A non-linear dynamic analysis of an eight-storey RC framed hospital building was firstly carried out to generate the floor acceleration time histories employed in the seismic analysis of the piping networks. The RC moment-resisting frame (Fig. 7) is characterized by nine bays at each floor in both principal directions. The inter-storey height and the bay length are equal to 3.4 m and 4.5 m, respectively. The properties of the RC frame elements were defined by simulated seismic design, according to Italian NTC 2018, [3]. A high seismic hazard zone (Benevento, Campania), a soil type A (intact hard) and a nominal life of the building equal to 100 years were assumed, as provided in NTC-18 [3] for hospitals. The design peak ground acceleration (PGA) corresponding to life-safety performance level (i.e return period equal to 949 years) is equal to 0.331 g. More details of the configuration of the building and the modelling approach are available in [18].

The seismic input employed for the analysis of the RC frame is composed of a set of 20 unscaled spectrum-compatible ground motions, selected from the European strong-motion database [36] using REXEL platform [37]. For each ground motion, the X, Y and Z components of the acceleration were applied in the three principal directions of the structure. The selected set was defined assuming 10% upper and lower deviation tolerance of matching between the average and the design spectrum. The so-defined criterion meets Eurocode 8 provisions [3,38]. The 5% damped elastic spectra of the selected ground motions, along with the design spectra and the fundamental period of the frame $\boldsymbol{T_{f1}}$, are provided in Fig. 8.

Even though the operation of the building is not required at LS performance level, the analysis at this stage might be useful for the damage assessment of the piping system in case of post-elastic response of the structure. Moreover, the stability assessment of NSCs at life-safety performance level is required in modern seismic design codes (e.g. [3]).

The floor response spectra (FRS) obtained for each of the principal direction at last floor are provided in Fig. 9. A significant amplification of the spectral acceleration response of the structure is observed, particularly in the vertical direction. As expected, the amplification range for floor spectral acceleration is narrower in the vertical direction compared to horizontal one. On the other hand, very close results were obtained comparing the two horizontal directions.

The seismic vulnerability of the piping systems analysed was assessed based on the damage rate of pipe joints and suspended piping seismic restraints, as well as on the maximum displacements of the network. The damage rate of each pipe joints was expressed as $\theta_{max}/\theta_{lim}$, where θ_{max} is the maximum rotation obtained from the analysis and θ_{lim} is the limit rotation.

The value of limit rotation is not necessarily equal to the ultimate rotation capacity of the joint prior failure. Particularly, referring to threaded steel joints employed in fire-fighting networks, leakage after the attainment of the yielding rotation, θ_y, was observed by Tian et al. [21], suggesting loss of operation before the attainment of the ultimate rotation. In case of medical gas distribution systems, local buckling of joints may represent a conservative loss of operation limit, because the distortion of the geometry of joints causes re-distribution of internal forces and possible low-cycle fatigue cracking. Hence, the value of θ_{lim} was set equal to θ_y and θ_b, for FP and MP joints, respectively, being θ_b the rotation corresponding to local buckling.

In case of suspended piping seismic restraints, the damage rate was computed as $\delta_{max}/\delta_{lim}$, being δ_{max} the maximum deformation of the braced restraints obtained from the analysis and δ_{lim} the yielding deformation. For the sake of clarity, the damage rate was expressed considering the maximum values of $\theta_{max}/\theta_{lim}$ and $\delta_{max}/\delta_{lim}$ computed among all the elements in the systems. Lastly, the maximum displacements ($\boldsymbol{D_{max}}$) at the nodes connected to suspended piping restraints were monitored.

3.2. Modal periods and participating mass ratios

An eigenvalue analysis was firstly performed, to identify the modes with higher influence on the dynamic response of the case study piping systems. As expected, several local modes were detected; hence, the highest values of participating mass ratio ($\boldsymbol{M}^*$) obtained for each degree of freedom (DOF) are firstly provided in Fig. 10. Additionally, the corresponding modal periods are reported in Table 3 and Table 4.

Both in case of MP and FP, the mode with highest participating mass ratio involves the translation of the main line along its longitudinal axis (MX in Fig. 10). Referring to the translation along the Y and Z axis (MY and MX, respectively) the highest value of $\boldsymbol{M}^*$ is lower than 40% for all the considered piping systems. This result is due to the presence of several local modes along Y and Z, with participating mass ratios ranging between 11% and 39%.

The variation of the dynamic behaviour comparing the two layouts is mainly evidenced by the higher $\boldsymbol{M}^*$, in Model B compared to Model A,

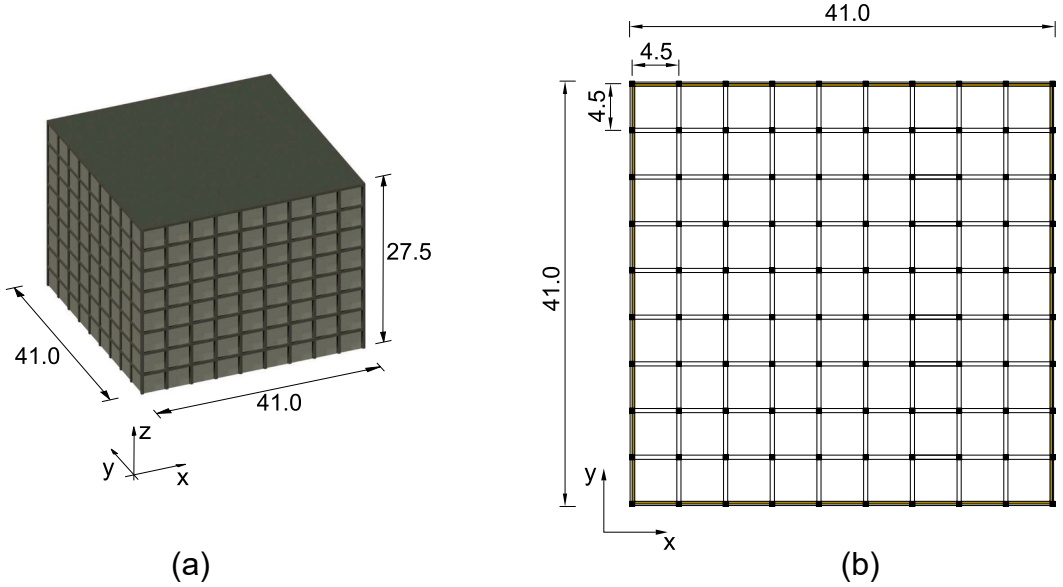

Fig. 7. 3D (a) and plan (b) configuration of the RC building analysed.

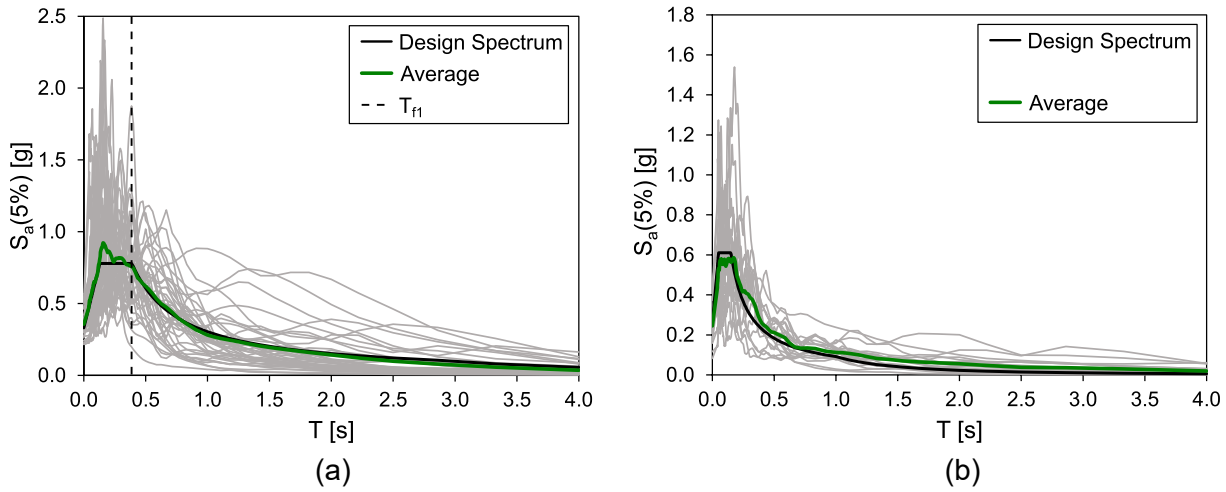

Fig. 8. (a) Horizontal and (b) vertical response spectra of the acceleration time histories considered for cascade analysis.

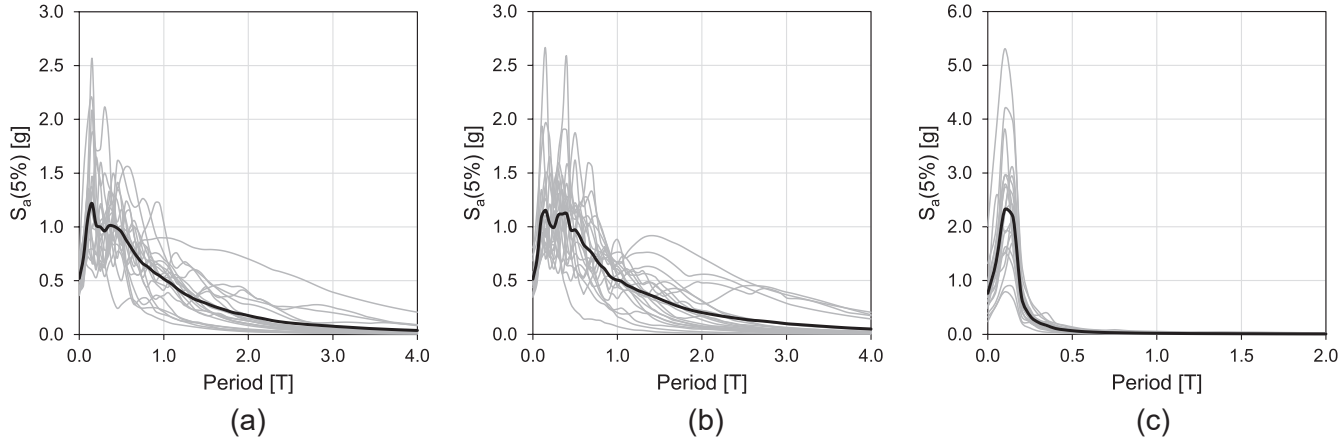

Fig. 9. Floor spectra obtained for (a) X, (b) Y and (c) Z direction.

for torsional local mode (RMZ in Fig. 10), alongside lower $\boldsymbol{M}^*$ for Y-translation mode. This outcome is related to the eccentricity between the centre of mass and stiffness, due to the eccentric location of both branch lines. Comparing the different configurations considered, higher $\boldsymbol{M}^*$ associated to the X-translation mode is observed as the number of pipes in the main line increases, except for C_2 in case of FP. Additionally, lower values of $\boldsymbol{M}^*$ for vertical translation mode were obtained comparing C_3 and C_4 to C_1 and C_2. This outcome is due to the decrease of the spacing between suspended piping seismic restraints, which reduces flexibility of the main line.

Referring to modal periods, lower values were generally obtained for local modes involving Z-translation, suggesting a possible amplification of the vertical floor acceleration. For Y-translation modes, a great difference is observed comparing MP to FP. In case of MP, the greater flexibility of the pipes leads to higher periods, suggesting minor spectral acceleration amplification. On the other hand, Y-translation modal periods are generally in the range corresponding to the highest amplification of spectral acceleration (Fig. 9**b**) in case of FP.

3.3. Influence of the vertical component on the performance

Considering the complexity of the piping systems' geometry, the influence of the interaction with the vertical component of the acceleration was firstly analysed. To this scope, the results obtained considering (Z accel ON) and neglecting (Z accel OFF) the vertical component of the acceleration in the analysis are compared. As said before, the resulting values of $\theta_{max}/\theta_{lim}$, $\delta_{max}/\delta_{lim}$ and $\boldsymbol{D}_{max}$, provided and discussed in the following refer to the maximum values computed among all the elements in the systems. For each parameter considered, the median value (solid line) alongside the Q1-Q3 (i.e. 1st and 3rd quartiles) ranges (dashed lines), computed among the results referred to the 20 floor acceleration inputs, are reported, depending on the configuration considered (i.e. the number of pipes in the main line). Only results referred to Model B are discussed in the following, since similar considerations apply to Model A. The results obtained for $\theta_{max}/\theta_{lim}$, in case of MP are illustrated in Fig. 11**a** and **b**, referring to main line and branch lines joints, respectively. For all the considered configurations, the value of $\theta_{max}/\theta_{lim}$ was significantly higher than one, resulting in a high seismic vulnerability of this type of pipe joints. Additionally, a great influence of the number of pipes in the main line was observed. The median value of $\theta_{max}/\theta_{lim}$ increases by 96% and 301% comparing C_1 to C_4 in case of main line and branch lines, respectively. On the other hand, negligible effect of the vertical component is detected. This outcome suggests a lower participating mass in the modes involving the vertical motion of the systems. Consequently, analyses conducted only considering the two horizontal components of the earthquake may adequately approximates the actual damage rate of pipe joints when subjected to tri-axial excitation.

The same considerations apply for the damage rate of suspended piping seismic restraints in MP (Fig. 12**a**). The median value of $\delta_{max}/\delta_{lim}$ increases by 494% comparing C_1 to C_4. Additionally, even if the median $\delta_{max}/\delta_{lim}$ is lower than 1.0 in all cases, the third quartile (Q3) is

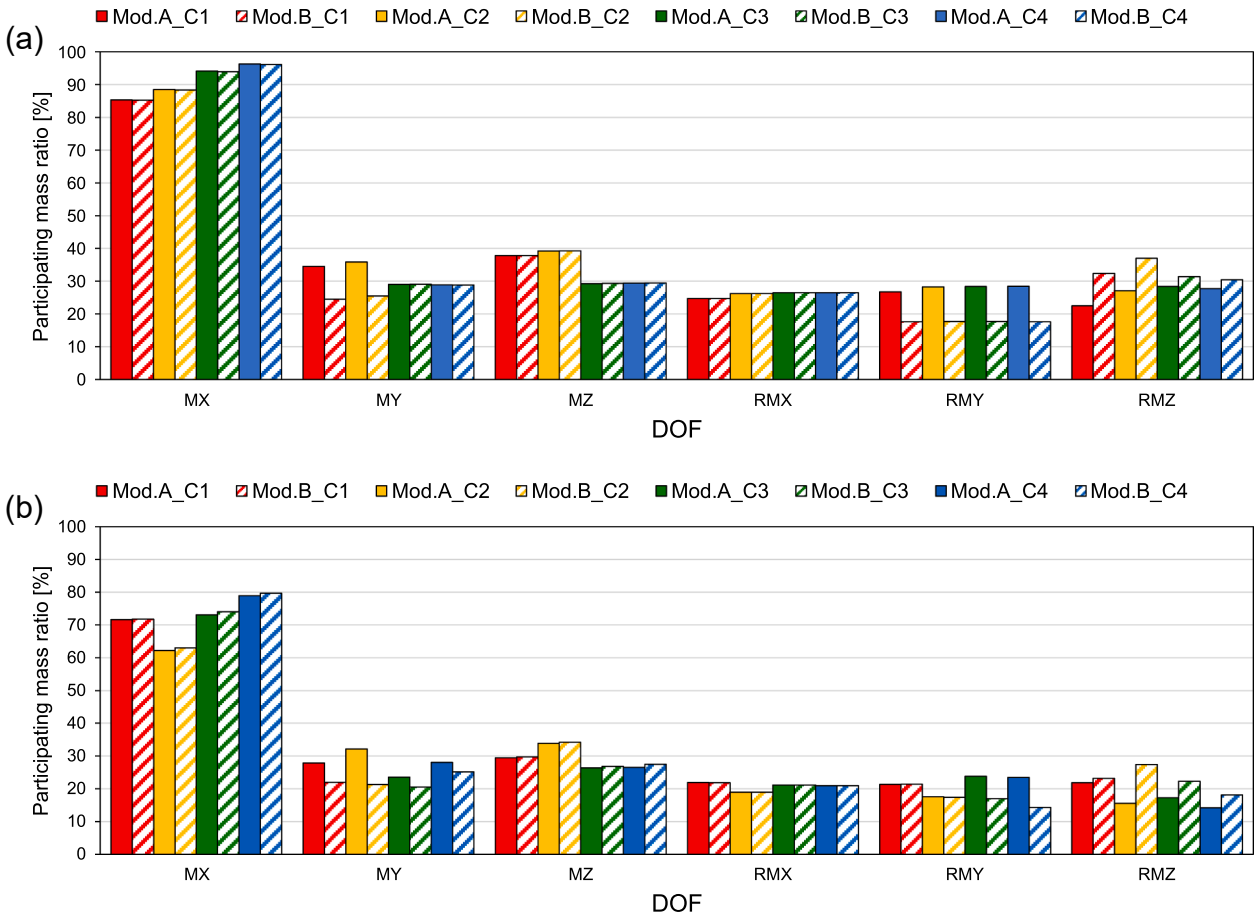

Fig. 10. Highest values of $\boldsymbol{M}^*$ for each DOF referring to (a) MP and (b) FP.

Table 3
Modal periods of modes with higher participating mass ratio at each DOF in case of MP.

	Model A				Model B			
DOF	**C_1**	**C_2**	**C_3**	**C_4**	**C_1**	**C_2**	**C_3**	**C_4**
MX	0.067	0.112	0.113	0.115	0.067	0.113	0.113	0.115
MY	1.195	2.014	0.068	0.070	1.314	2.215	0.068	0.070
MZ	0.013	0.021	0.009	0.027	0.013	0.021	0.026	0.027
RMX	0.002	0.002	0.002	0.002	0.002	0.002	0.002	0.002
RMY	0.011	0.018	0.023	0.023	0.011	0.018	0.023	0.023
RMZ	2.463	4.151	5.066	4.994	2.449	4.127	4.962	4.751

Table 4
Modal periods of modes with higher participating mass ratio at each DOF in case of FP.

	Model A				Model B			
DOF	**C_1**	**C_2**	**C_3**	**C_4**	**C_1**	**C_2**	**C_3**	**C_4**
MX	0.082	0.119	0.119	0.120	0.082	0.118	0.119	0.120
MY	0.342	0.483	0.251	0.184	0.038	0.538	0.262	0.189
MZ	0.017	0.024	0.028	0.028	0.017	0.024	0.028	0.028
RMX	0.007	0.007	0.007	0.007	0.007	0.007	0.007	0.007
RMY	0.007	0.021	0.024	0.025	0.017	0.024	0.024	0.024
RMZ	0.038	2.175	2.256	1.740	2.440	3.450	2.488	1.793

equal to 1.23 and 1.25 for C_3 and C_4, respectively. On the one hand, this outcome suggests that the adoption of equivalent static approaches for the seismic design of suspended piping restraints may be adequate even for complex piping systems. However, unconservative estimation of the seismic demand could be obtained, since the presence of multiple pipes in main lines may lead to uneven distribution of lateral forces.

In some cases, lower values of median $\theta_{max}/\theta_{lim}$ were obtained considering the vertical acceleration. Such not-intuitive result may be due to the post-elastic response in vertical direction, related to pipe joints damage. This fashion causes reduction of the stiffness of the network in both horizontal and vertical direction, leading to lower seismic demand.

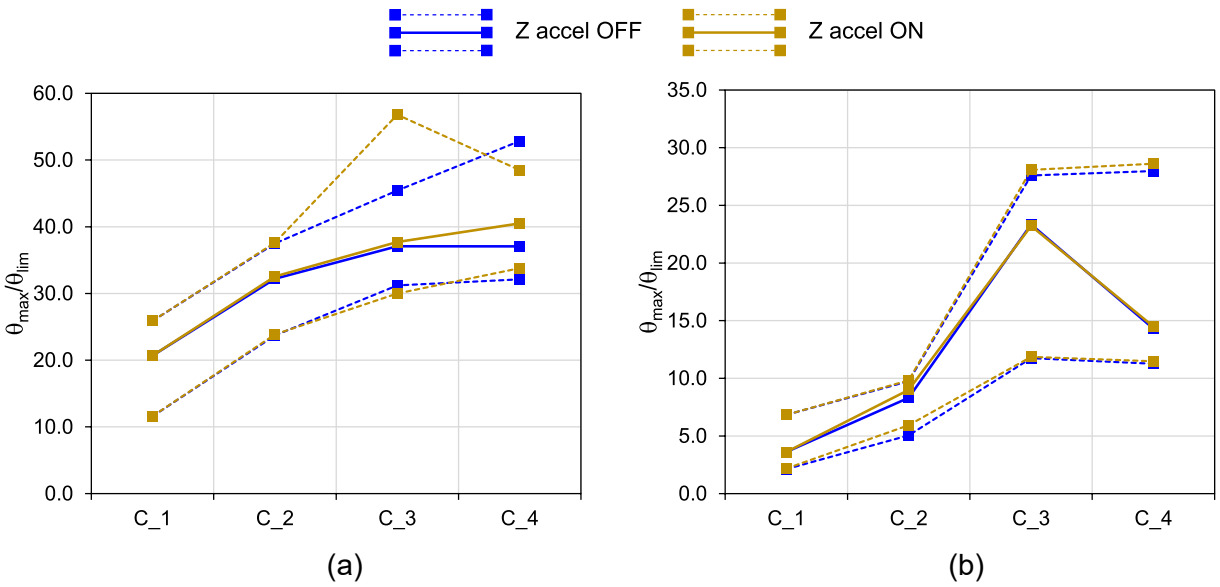

Fig. 11. Comparison of the maximum $\theta_{max}/\theta_{lim}$ at (a) main line and (b) branch lines joints obtained for all Model B configurations of MP considering and neglecting the vertical component of the seismic action.

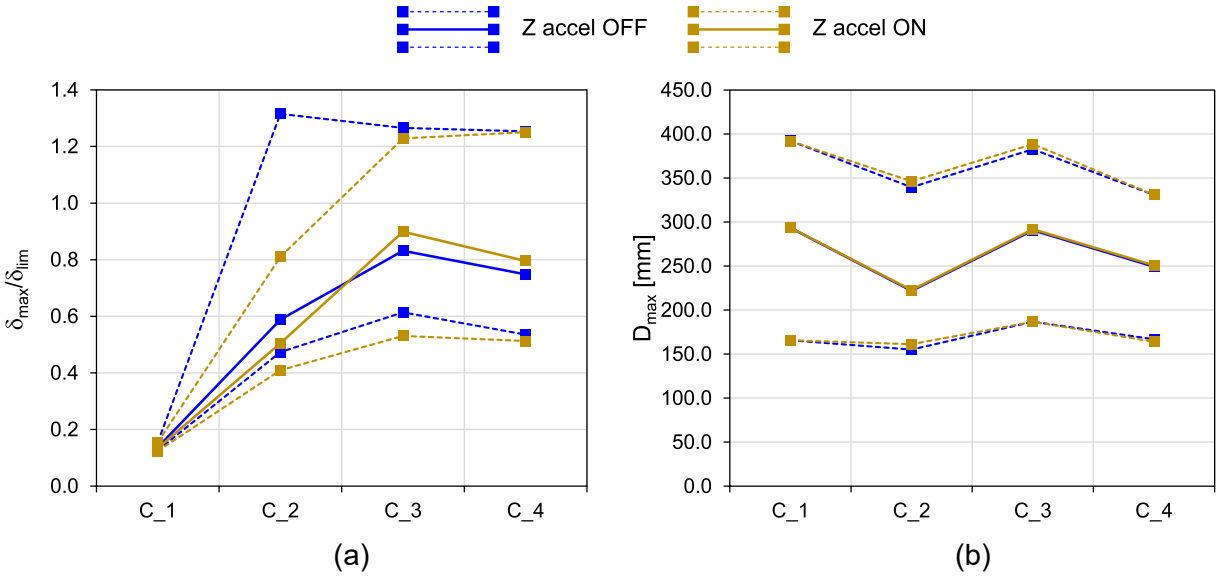

Fig. 12. Comparison of the maximum (a) $\delta_{max}/\delta_{lim}$ and (b) $\boldsymbol{D}_{max}$ obtained for all Model B configurations of MP considering and neglecting the vertical component of the seismic action.

Referring to the maximum displacements ($\boldsymbol{D}_{max}$) of the MP system (Fig. 12**b**), negligible effect of the vertical component on the results was obtained, similarly to $\theta_{max}/\theta_{lim}$ and $\delta_{max}/\delta_{lim}$. On the other hand, the influence of the mass in the main line doesn't have a clear trend. This result is due to the balance between the decrease of spacing between seismic restraints and the increase of the mass as the number of pipes in the main lines increases.

The results of $\theta_{max}/\theta_{lim}$ obtained for FP system are provided in Fig. 13. A noticeable influence of the vertical component of the seismic acceleration on the resulting median values is observed in this case. This outcome is probably caused by the greater participating mass associated to the modes involving vertical translation of the main line.

A significantly lower influence of the number of pipes in the main line on the value of $\theta_{max}/\theta_{lim}$ in branch lines' joints is observed compared to MP. The average $\theta_{max}/\theta_{lim}$ increases by 93% and 31% for main line and branch lines joints, respectively, comparing C_4 to C_1. This result is probably caused by the higher flexural stiffness of pipe joints in FP, which leads to a more uniform distribution of internal forces in the pipes. Additionally, it is worth noting that the median value of θ_{max} obtained for FP was lower than the yielding rotation for all the considered floor accelerograms, both in case of main line and branch lines' pipe joints. Hence, loss of operation of the system was not attained due to absence of yielding.

The results referred to $\delta_{max}/\delta_{lim}$ in FP systems are provided in Fig. 14**a**. Differently from MP results, greater damage rate was obtained in seismic restraints compared to pipe joints in this case. The value of $\delta_{max}/\delta_{lim}$ was, indeed, higher than 1.0 for almost all configurations. Moreover, the presence of pipe joints with higher stiffness with respect to MP led to a more uniform distribution of lateral forces on seismic restraints. Hence, a lower increase of $\delta_{max}/\delta_{lim}$ for higher number of pipes in the main lines (+340% comparing C_1 to C_4) was observed compared to MP. On the other hand, a similar trend is observed in

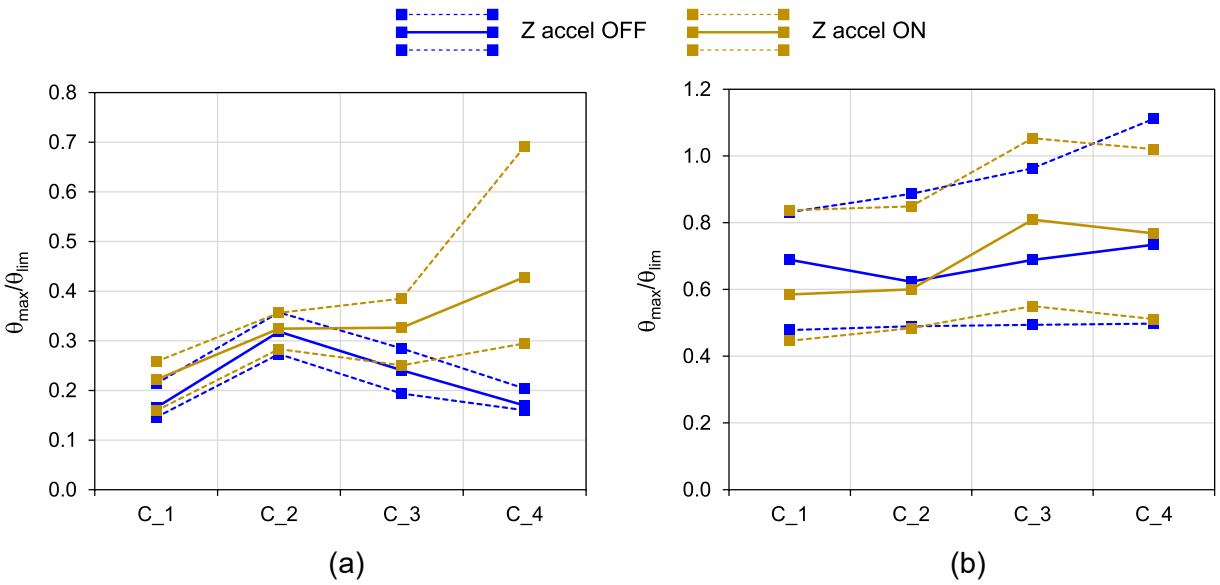

Fig. 13. Comparison of the maximum $\theta_{max}/\theta_{lim}$ at (a) main line and (b) branch lines joints obtained for all Model B configurations of FP considering and neglecting the vertical component of the seismic action.

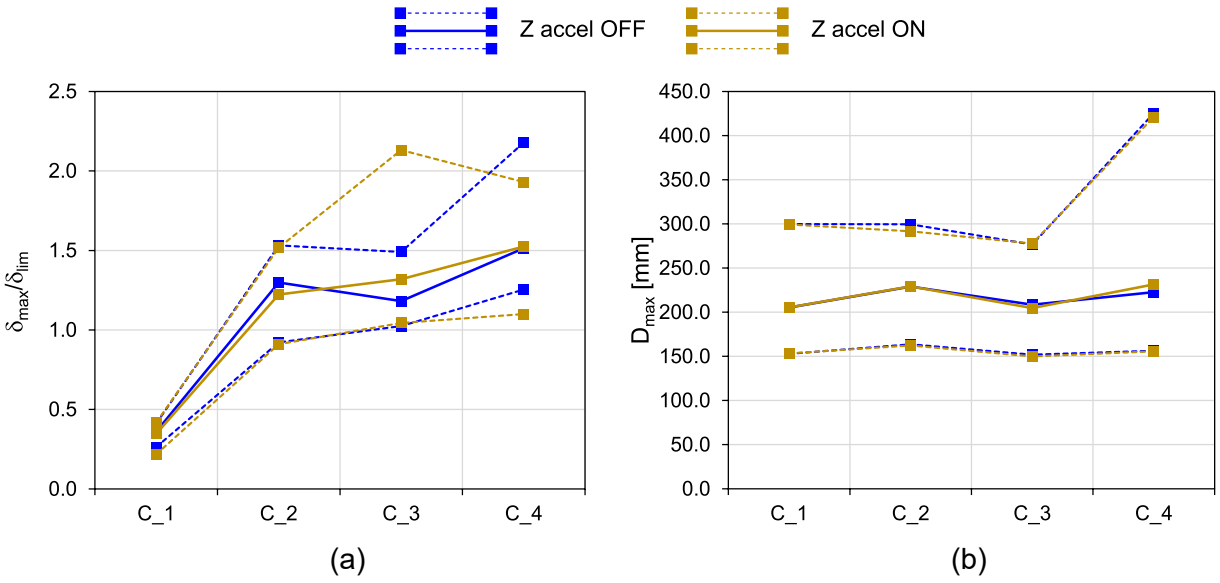

Fig. 14. Comparison of the maximum (a) $\delta_{max}/\delta_{lim}$ and (b) D_{max} obtained for all Model B configurations of FP considering and neglecting the vertical component of the seismic action.

Fig. 12**a** and Fig. 14**a**. Lastly, the results referred to the maximum displacement D_{max} of the piping systems are illustrated in Fig. 14**b**. Similarly to MP, the negligible effect of the vertical component on the results is due to the lower spacing between seismic restraints and the increase of the mass as the number of pipes in the main lines increases.

3.4. Influence of the geometry on the performance

In order to analyse the effect of the geometry of the network on the performance of the piping systems, the results referred to Model A and Model B, are compared in the following. Fig. 15 reports the results of $\theta_{max}/\theta_{lim}$ for main and branch lines' pipe joints (Fig. 15**a** and Fig. 15**b**, respectively) in case of MP. The difference between the response of Model A and Model B seems not clearly influenced by the number of pipes on the main line. This result suggests the hardships in providing general statements regarding the seismic response of such piping systems, because of the high variability of the influence of higher modes.

In the case of branch lines joints (Fig. 15**b**), higher damage was generally observed in case of Model A, even though the great variability of the results hinders a proper interpretation. The average value of $\theta_{max}/\theta_{lim}$ reduced by 46%, 16%, 21% and 49% comparing Model B to Model A. This outcome might be caused by the higher effects of torsional modes in Model B, due to the irregular geometry. Consequently, the relative translation between main and branch lines is reduced, leading to lower rotation of branch lines joints.

Referring to suspended piping seismic restraints, similar response was observed comparing Model B to Model A (Fig. 16**a**), except for the case C_3. Also in this case, the reason of this specific outcome might be the torsional motion obtained in Model B, which amplifies the deformation of eccentric suspended piping seismic restraints. However, it is worth mentioning that the great variability of the results hinders their comprehensive interpretation also in this case. Lastly, no significant

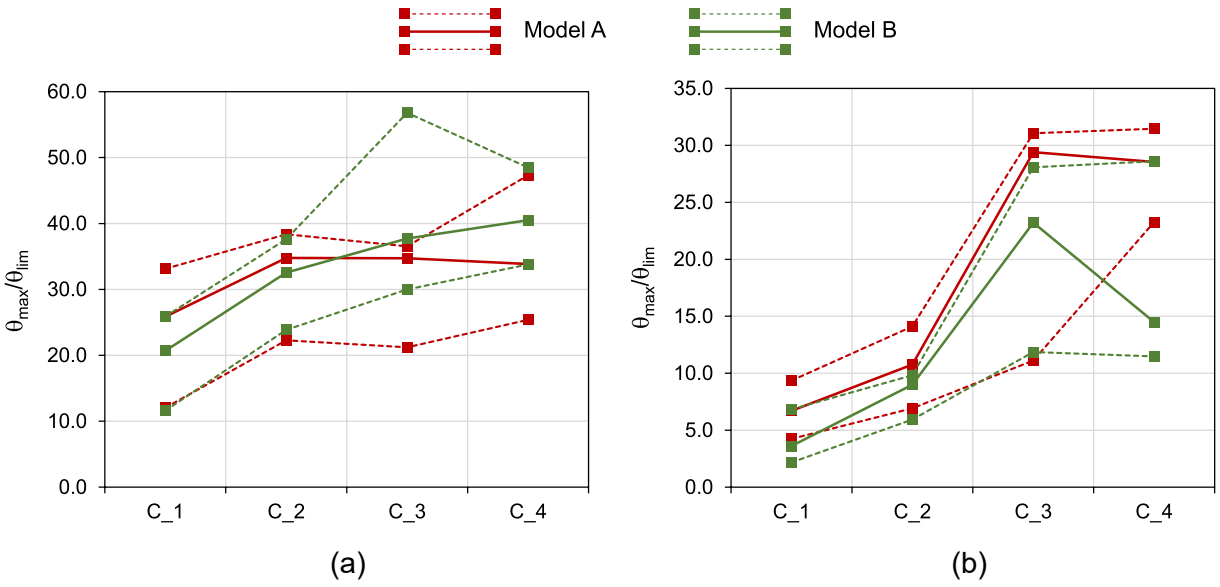

Fig. 15. Comparison of the maximum $\theta_{max}/\theta_{lim}$ at (a) main line and (b) branch lines joints obtained for all configurations of MP in case of Model A and Model B.

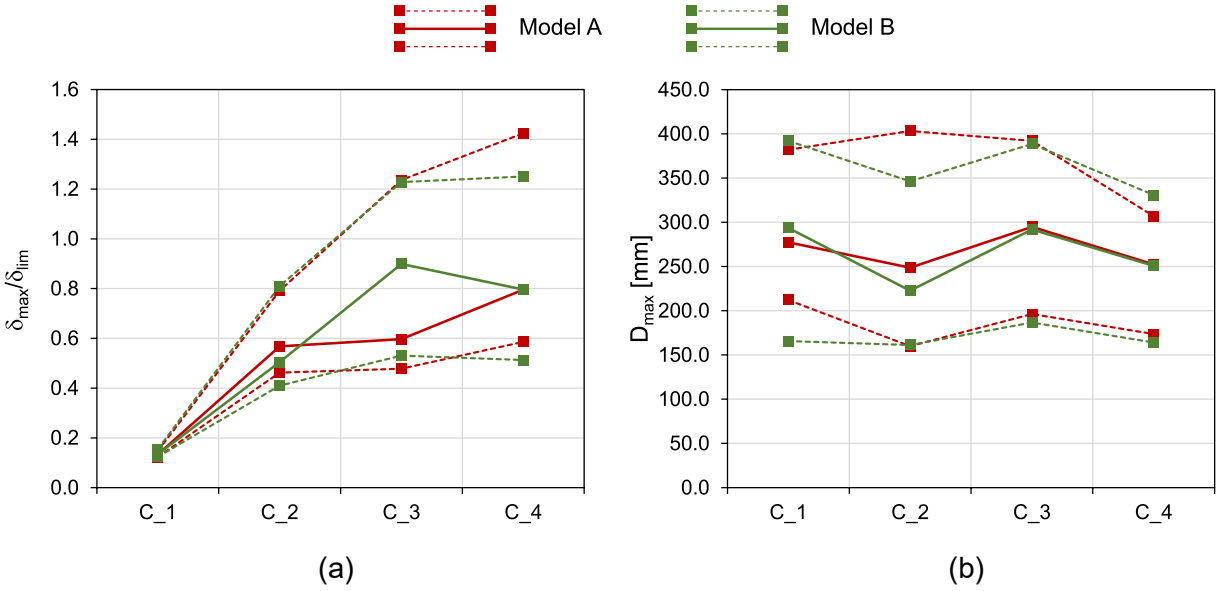

Fig. 16. Comparison of the maximum (a) $\delta_{max}/\delta_{lim}$ and (b) D_{max} obtained for all configurations of MP in case of Model A and Model B.

influence of the geometry of the system on the maximum displacements is detected, as shown in Fig. 16**b**. This result confirms the relevance of local modes on the seismic response of the piping layout, which leads to different relative displacements/deformations comparing Model A to Model B, although the absolute displacements are not significantly affected.

The results obtained in case of FP systems are reported in Fig. 17 and Fig. 18. A significantly higher damage rate on main lines pipe joints is observed in case of Model A with respect to Model B. The average $\theta_{max}/\theta_{lim}$ increased by 197%, 62%, 94% and 231% in case of C_1, C_2, C_3 and C_4, respectively, comparing Model A to Model B. This outcome may be caused by higher participating mass in local modes involving transverse translation of the main line, which led to noticeable relative rotation of joints with respect to branch lines.

Referring to branch lines joints (Fig. 17**b**), a lower difference between damage rate in Model A and Model B is detected compared to main lines joints, because the low mass of the branch lines led to negligible relative motion with respect to the main line. On the other hand, the position of the branch line seems to significantly affect the maximum rotation at the joint in case of C_2, for which $\theta_{max}/\theta_{lim}$ was 39% higher in Model A compared to Model B. However, this specific outcome was likely obtained because of the peculiar interaction between local modes and the seismic input.

Referring to $\delta_{max}/\delta_{lim}$, no significant influence of the position of the branch lines on the results was observed (Fig. 18**a**), since both average values and Q1-Q3 ranges are similar for each configuration considered. It is worth noting the different values of $\delta_{max}/\delta_{lim}$ obtained varying the number of pipes in the main line. Particularly, a great difference is obtained in C_1 compared to the remaining cases. This fashion is due to the adoption of the maximum allowed spacing between restraints in C_1, according to provisions by NFPA 13 [29], instead of the result of equation (1). Consequently, a lower exploitation of the restraints was obtained in this case. On the other hand, similar values were obtained for C_2, C_3 and C_4, in which the restraints' spacing varied depending

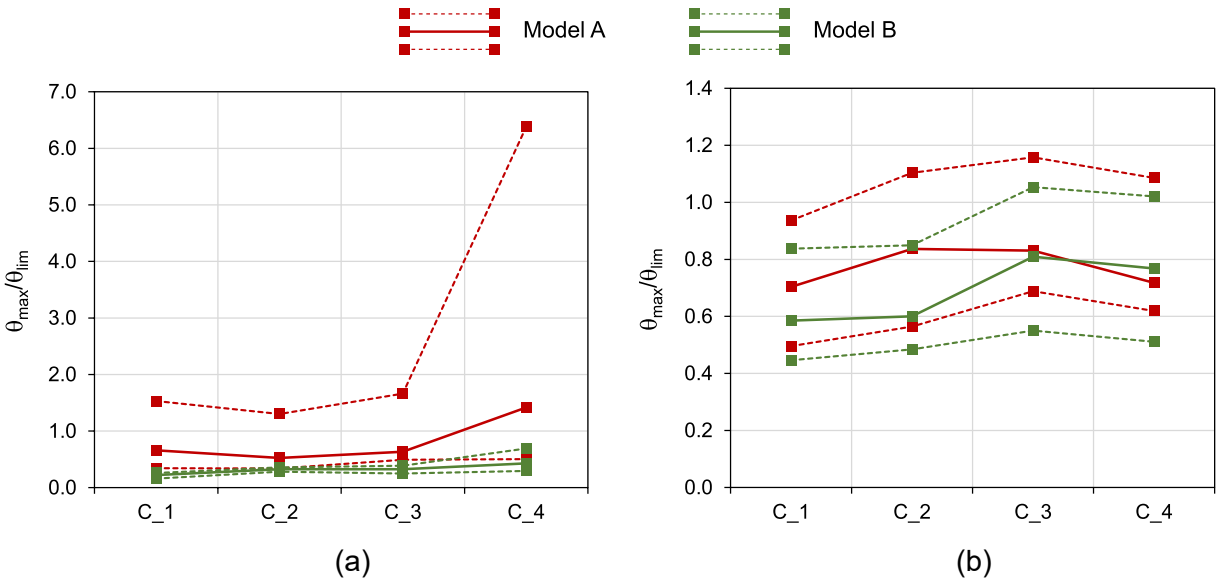

Fig. 17. Comparison of the maximum $\theta_{max}/\theta_{lim}$ at (a) main line and (b) branch lines joints obtained for all configurations of FP in case of Model A and Model B.

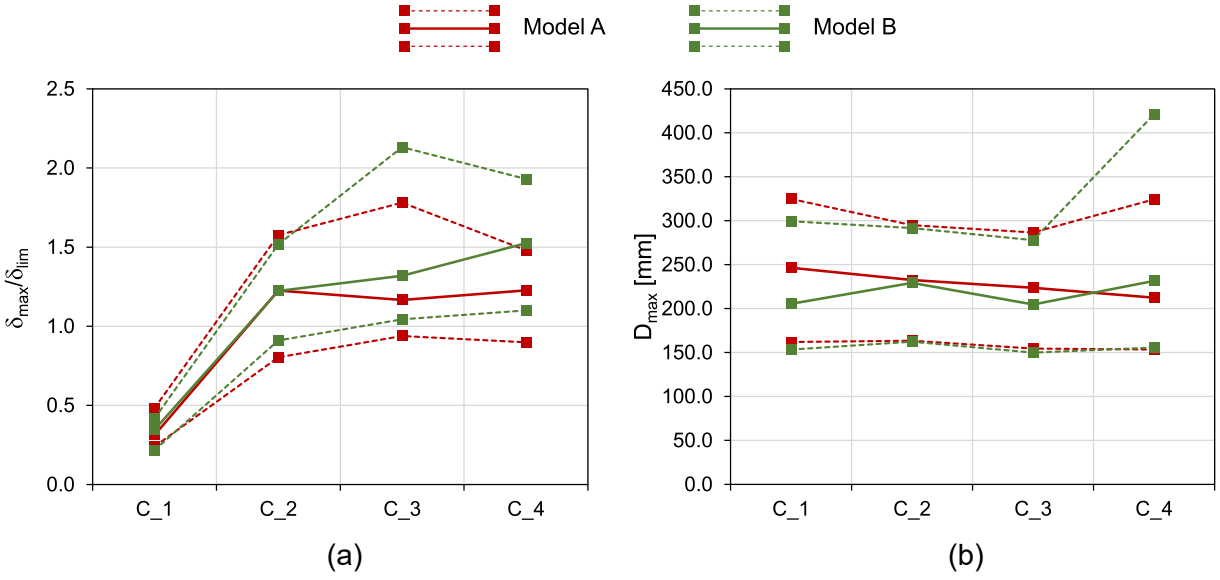

Fig. 18. Comparison of the maximum (a) $\delta_{max}/\delta_{lim}$ and (b) $\boldsymbol{D_{max}}$ obtained for all configurations of FP in case of Model A and Model B.

on the number of pipes in main line. This aspect evidences that equivalent static approaches (such as [3,27,28]), assuming the demand on the seismic restraint being linearly proportional to the mass of the pipe line, might be suitable also for complex networks. Furthermore, the maximum deformation obtained in case of C_2, C_3 and C_4 was not significantly higher than yielding deformation, confirming the previous statement.

Lastly, the results obtained for the maximum displacement $\boldsymbol{D_{max}}$ of the FP systems are reported in Fig. 18**b**. The same considerations regarding MP systems apply in this case. In fact, the response of the networks was highly influenced by local modes also for FP systems, resulting in a great difference in relative displacements/deformations rather than absolute displacements comparing Model A to Model B.

As said before, the complex configuration of the piping networks led to uneven distribution of internal forces, causing localized failure of pipe joints. Fig. 19 is provided as an example to confirm the previous statements, showing the average values of $\theta_{max}/\theta_{lim}$ obtained for Model A in case of MP and FP.

Each joint is identified with an ID, expressing the pipe line where it is located (ML = main line, BL = branch line) and numbered starting from the left end of the main line (Fig. 1). For both MP and FP, the vertical rotation was generally lower than the horizontal rotation, suggesting the negligible effect of vertical acceleration on maximum damage. The highest rotation was generally obtained at ML1, due to the horizontal translation of the first span in main line, which was not restrained with braced connections.

Aiming to emphasize the significant difference between MP and FP response, Fig. 20 provides a summary of the results obtained for Model A. Also in this case, the reported $\theta_{max}/\theta_{lim}$, $\delta_{max}/\delta_{lim}$ and $\boldsymbol{D_{max}}$ are the median values computed among the 20 input motions. The great difference in terms of pipe joint damage, due to the different materials employed for pipes, is evidenced in Fig. 20**a** and **b**, confirming the high vulnerability of MP from a loss of operation standpoint. On the other hand, higher damage rate was detected for seismic restraints in case of FP compared to MP (Fig. 20**c**), due to the greater mass of the system. Lastly, the type of the system seems not to influence the maximum

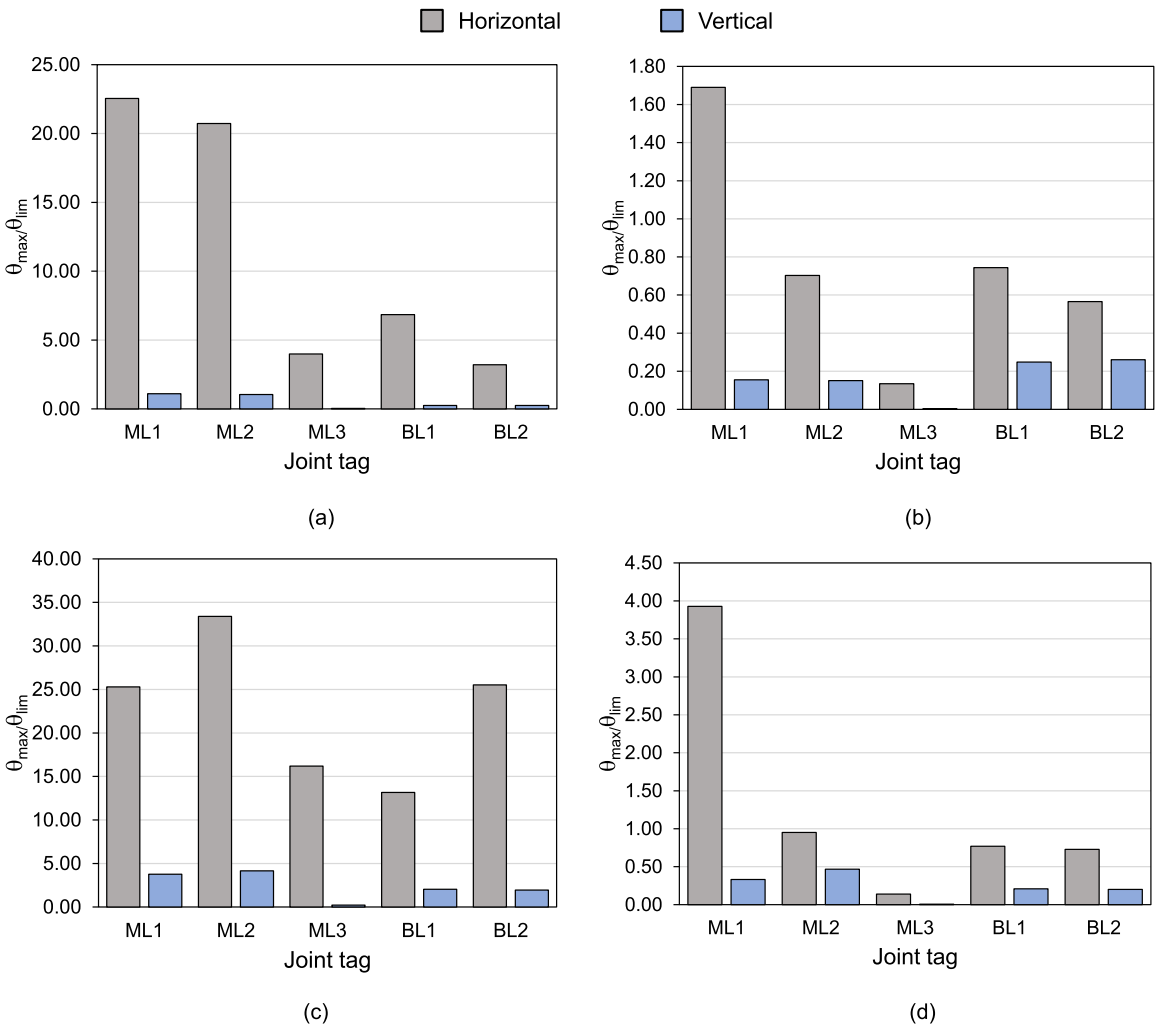

Fig. 19. Average values of of maximum damage rate obtained for all pipe joints in the network, in case of (a) C_1 for MP, (b) C_1 for FP (c) C_4 for MP and (d) C_4 for FP (results referred to Model A).

displacements, as shown in (Fig. 20**d**).

4. Fragility functions

The parametric study performed allowed to identify the influence of several parameters on the seismic response of piping systems. Particularly, the peculiarity of the interaction between local modes and floor acceleration time-history was evidenced. This aspect leads to hardships in providing general statements regarding the effect of the geometry of the network on the seismic vulnerability. On the other hand, a clear correlation between the mass of the main line and the seismic demand on suspended piping seismic restraints and pipe joints was observed.

Aiming to provide a more accurate estimation of the seismic vulnerability on such NSCs, incremental dynamic analyses (IDA, [39]) were performed on all the configurations considered in this study, to compute fragility functions depending on the parameters analysed. The incremental dynamic analyses were carried out by progressively scaling each of the 20 tri-directional floor accelerograms through a non-negative factor $\lambda_{IDA} \in [0; +\infty)$, up to the achievement of a specific performance level (PL) of the piping system. This approach neglects the modification of the filtering effect of the structure, due to non-linear response, as the ground motion intensity increases. Considering the importance of such piping systems, two PL were considered for the IDA, namely operation-limit and life-safety. The attainment of the operation-limit PL was assumed once leakage at pipe joints occurred (i.e. $\theta_{max}/\theta_{lim} > 1.0$). Referring to life-safety PL, a reasonable limit state assumption could be the collapse of a pipe line in the network. This event was related to either collapse of seismic restraints or pipe joints.

Based on the IDA results, the fragility functions were computed by fitting the values of peak floor acceleration (PFA) either at operation limit or collapse of the system, obtained for each ground motion through log-normal cumulative density functions (CDF). Despite Spectral acceleration is generally used for such applications, the great influence of higher modes hindered identifying a mode with significant participating mass ratio for the analysed systems. The CDF were calibrated through the maximum likelihood estimate for the mean and the standard deviation. The resulting values of the median PFA ($\boldsymbol{PFA_m}$) and the logarithmic standard deviation (σ_{log}) referred to each fragility function are reported in Table 5.

The fragility functions obtained at operation-limit PL for MP systems are provided in Fig. 21, in case of Model A and Model B, respectively. For both configurations, a clear influence of the mass of the main line on the vulnerability is observed, confirming the results obtained in previous sections. However, no significant variation is observed comparing C_3 to C_4. The reduction of spacing between seismic restraints, due to the increase of main line's mass, reduced flexibility of the pipes. At the same time, greater influence of modes involving the translation of main line cause higher rotation at pipe joints.

Referring to life-safety PL (Fig. 22), the collapse of the system was related to seismic restraints failure for all the considered cases. A

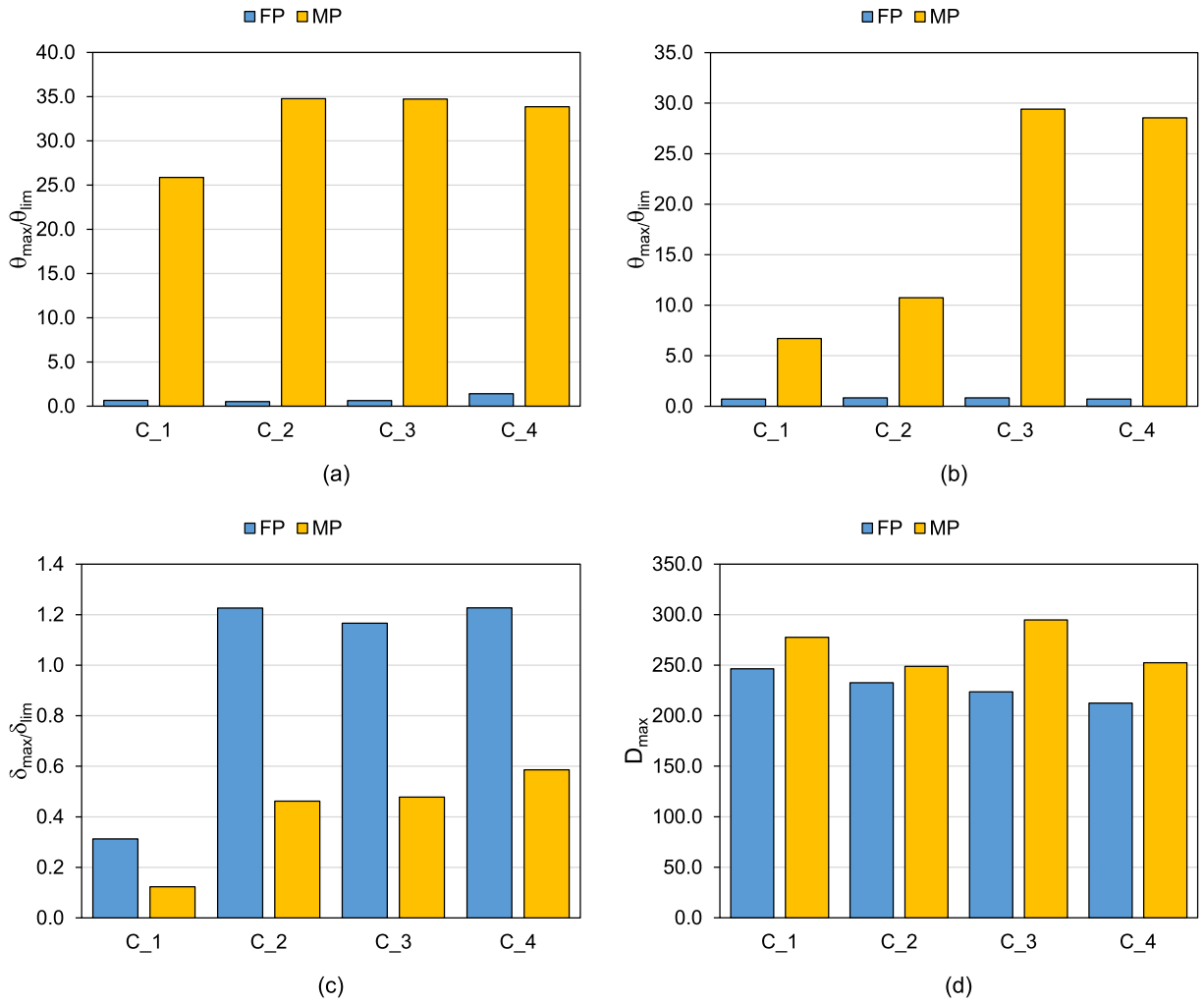

Fig. 20. Comparison between MP and FP response in case of Model A, referring to (a) $\theta_{max}/\theta_{lim}$ for main line joints, (b) $\theta_{max}/\theta_{lim}$ for branch lines joints, (c) $\delta_{max}/\delta_{lim}$ and (d) D_{max}.

Table 5
Obtained values of PFA_m and σ_{log} for all the considered cases.

			Model A				Model B			
	PL		C_1	C_2	C_3	C_4	C_1	C_2	C_3	C_4
MP	*DL*	PFA_m [g]	0.156	0.100	0.054	0.047	0.246	0.168	0.065	0.059
		σ_{log}	0.577	0.570	0.527	0.447	0.427	0.504	0.489	0.482
	LS	PFA_m [g]	2.517	0.868	0.772	0.687	2.398	0.846	0.704	0.627
		σ_{log}	0.379	0.413	0.398	0.362	0.428	0.421	0.392	0.439
FP	*DL*	PFA_m [g]	0.938	0.513	0.655	0.544	0.947	0.617	0.637	0.546
		σ_{log}	0.348	0.375	0.341	0.386	0.245	0.366	0.330	0.348
	LS	S_{am} [g]	1.178	0.574	0.618	0.600	1.256	0.593	0.611	0.530
		σ_{log}	0.356	0.416	0.351	0.405	0.371	0.359	0.335	0.402

significantly higher performance was obtained in case of C_1 compared to the remaining configurations. This result is likely caused by the design approach employed for suspended piping seismic restraints. In fact, the maximum allowed spacing between restraints was adopted both for C_1 and C_2, according to provisions by NFPA 13 [29], regardless of the results of equation (1).

Consequently, the mass increase in C_2 led to significantly higher demand on the seismic restraints compared to C_1. Referring to the remaining configurations, the increase of the mass in the main line was balanced by the reduction of the restraints' spacing, leading to similar results as the mass increases.

In case of FP, a similar trend of the results was obtained compared to MP at operation-limit PL. In fact, a clear influence of the mass of the main line on the vulnerability of the system is evidenced in both Model A and Model B (Fig. 23**a** and **b**). On the other hand, significantly higher performances were obtained for FP, for which the median PFA was 268–1105% higher compared to MP. This outcome is related to the higher flexural strength of threaded steel joints with respect to welded copper joints employed in MP.

Referring to life-safety PL (Fig. 24**a** and **b)**, the higher mass of FP with respect to MP caused an increase of vulnerability, due to the higher demand on suspended piping seismic restraints. In case of Model A, the reduction of PFA at life-safety performance level in FP compared to MP was equal to 53%, 34%, 20%, 13% for C_1, C_2, C_3 and C_4,

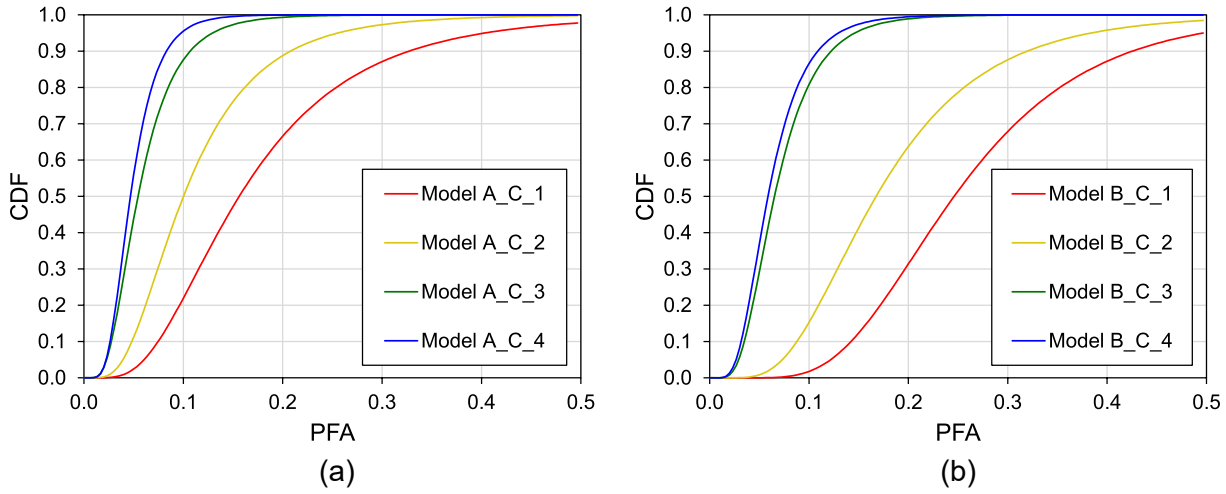

Fig. 21. Fragility functions for MP at operation-limit performance level in case of (a) Model A and (b) Model B.

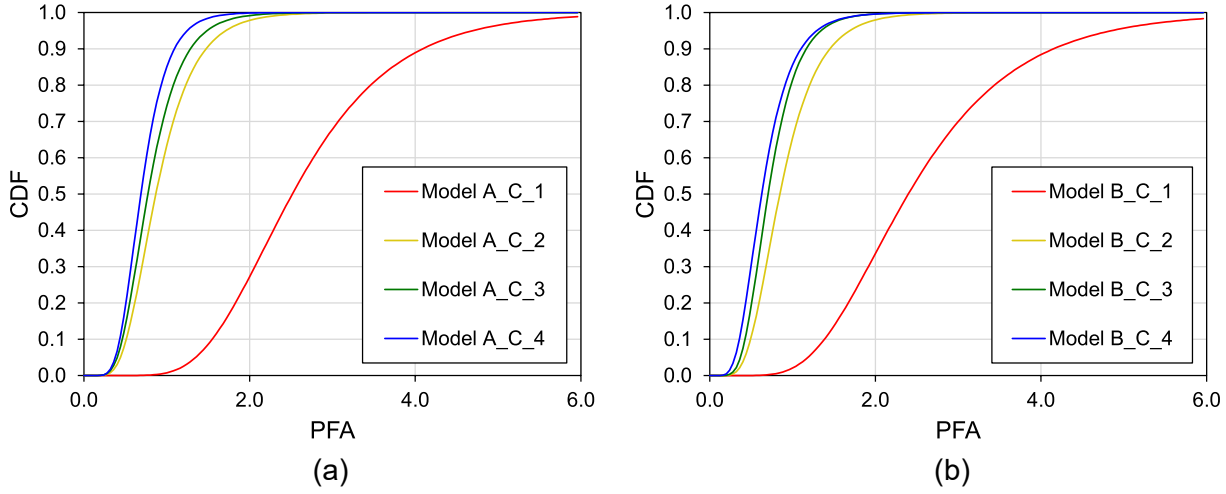

Fig. 22. Fragility functions for MP at life-safety performance level in case of (a) Model A and (b) Model B.

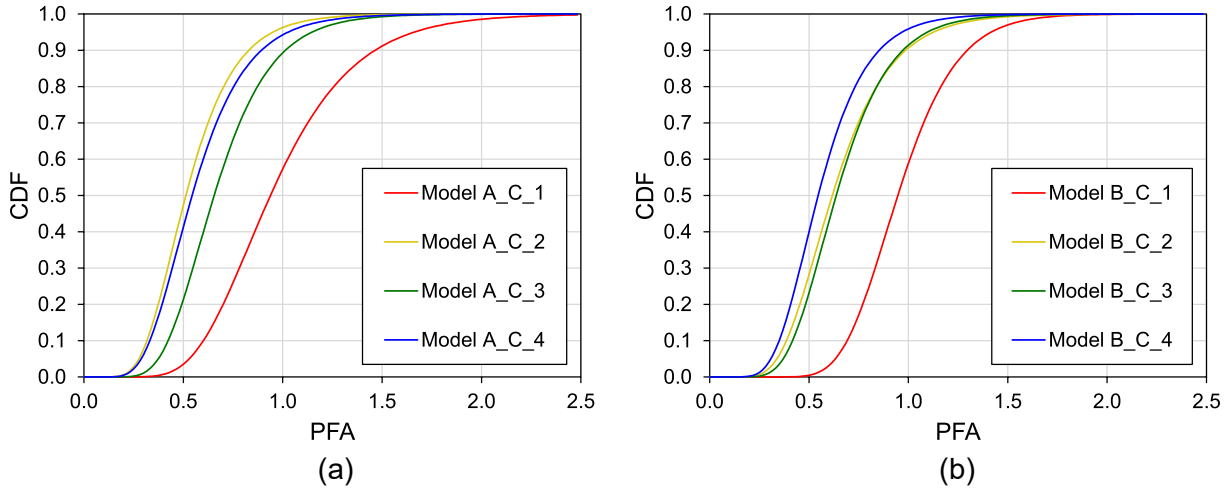

Fig. 23. Fragility functions for FP at operation-limit performance level in case of (a) Model A and (b) Model B.

respectively. Referring to Model B, the PFA at life-safety PL was 48%, 30%, 13%, 15% lower in FP compared to MP for C_1, C_2, C_3 and C_4, respectively.

It should be evidenced that the additional pipes included in the main line were identical in FP and MP. Hence, the influence of the mass of either MP or FP line on the total mass reduced by increasing the number

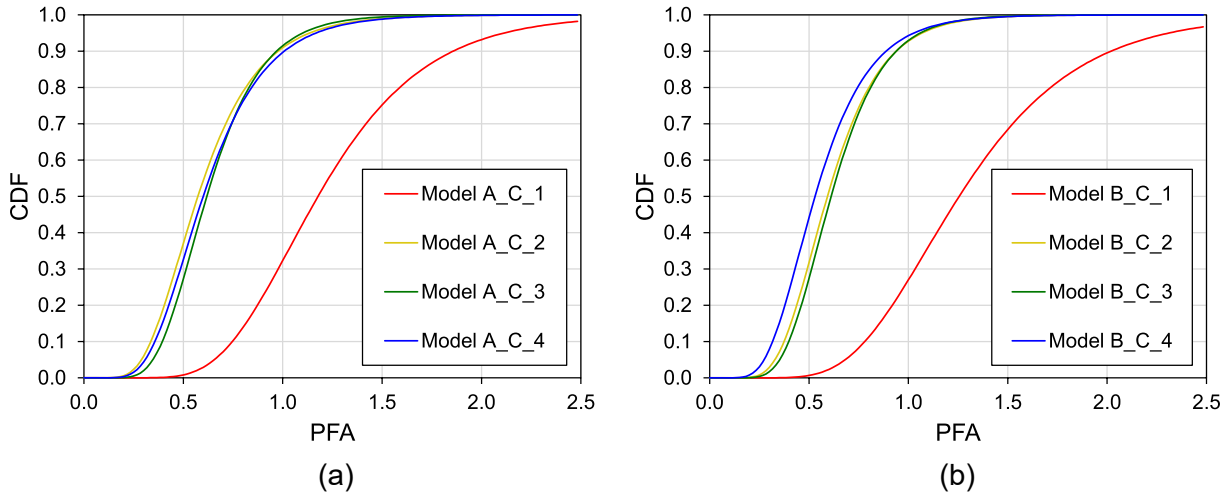

Fig. 24. Fragility functions for FP at life-safety performance level in case of (a) Model A and (b) Model B.

of pipes in the main line. Consequently, the results obtained were closer in case of C_4 comparing FP to MP.

The different response observed comparing MP to FP performance is evidenced in Fig. 25, which provides fragility functions obtained at DL and LS in case of Model A for C_3. This specific case was considered as example to highlight several aspects, addressed in the following.

Firstly, the influence of the material used for pipes and pipe joints is higher at DL performance level, because early local buckling of copper pipes leads to significantly higher vulnerability of MP compared to FP. On the other hand, the lower mass of MP causes lower seismic restraints' damage and, consequently, higher global performance at LS with respect to FP. Lastly, it is worth noting the close values of $\boldsymbol{PFA}_{\boldsymbol{m}}$ comparing DL to LS in case of FP. In fact, high flexural strength of pipe joints causes loss of operation occurring for a seismic demand close to that referred to seismic restraints' failure.

5. Conclusions

The cascade analysis performed in this study was aimed at assessing the influence of several parameters on the vulnerability of two types of piping systems. The dynamic response of the systems was accurately simulated by modelling non-linear behaviour of suspended piping restraints and pipe connections. The utilized model allowed to analyse the mechanical damage and the loss of operation of the systems due to earthquake.

The main outcomes of the study are listed pointwise in the following.

- The effect of the vertical acceleration on the damage rate seems negligible for both medical gas and fire-fighting piping system in all the configurations considered. On the other hand, the high variability of the results, as well as the peculiarity of the geometry of such non-structural components, suggests the need of deeply investigating the possible interaction between local modes and vertical component. Additionally, the influence of the type of conveyed fluid on the dynamic performance should be examined, by developing more complex micro- or meso-models.
- The results of the numerical simulation showed an influence of the geometry of the layout on the maximum pipe joints' rotations and the maximum displacements. The position of branch lines influenced the occurrence of pipe-joint yielding/buckling in case of high number of pipes in the main line, because of the different participating mass in local modes.
- For the analysed cases, the geometry of the layout seems to have negligible influence on seismic restraints damage. On the other hand, a clear dependency between seismic restraints damage and mass of the main line was detected. This is the consequence of the prescriptive requirements adopted in terms of maximum spacing between seismic restraints, which often rules their seismic design in case of light systems.

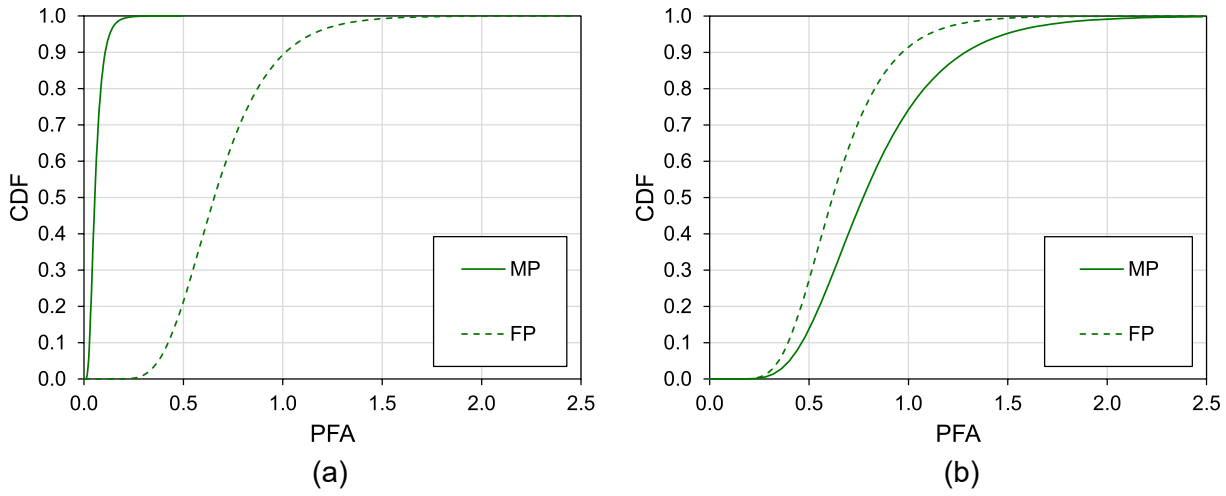

Fig. 25. Comparison between MP and FP fragility functions at (a) DL and (b) LS, in case of Model A and C_3.

- Fragility functions suggest satisfactory performance at both life safety and operation limit performance level in case of light piping systems. Particularly, the vulnerability of pipe joints was significantly lower when reducing the number of pipes in the main lines, even though higher seismic restraints' spacing was assumed.
- The type of the system and, consequently, the type of material adopted for pipes and joints, highly influenced the operation limit performance level. The higher strength of joints in fire-fighting networks compared to medical gas distribution networks significantly increased peak floor acceleration at loss of operation. On the other hand, lower peak floor acceleration at collapse of suspended piping seismic restraints was obtained in fire-fighting systems, due to their greater mass.

The results obtained in this paper evidence that simplified approaches may be reliable for the design of seismic restraints regardless of the geometry of the layout. However, local modes may lead to noticeable variation of the damage on pipe joints and, consequently, on the operation of the piping system. Additionally, the geometry of the layout was found to influence the seismic demand, particularly in case of high number of pipes in main line. Some aspects were not considered in this work and need further investigation, such as the presence of different types of gravity and seismic restraints and the presence of vertical necks, which may significantly affect maximum displacements/joint rotations due to earthquake action.

CRediT authorship contribution statement

Gianni Blasi: Conceptualization, Methodology, Software, Validation, Formal analysis, Investigation, Resources, Data curation, Writing – original draft, Writing – review & editing, Visualization. **Daniele Perrone:** Conceptualization, Methodology, Resources, Data curation, Writing – original draft, Writing – review & editing, Visualization, Supervision. **Maria Antonietta Aiello:** Conceptualization, Resources, Writing – original draft, Writing – review & editing, Visualization, Supervision.

Declaration of Competing Interest

The authors declare that they have no known competing financial interests or personal relationships that could have appeared to influence the work reported in this paper.

Data availability

Data will be made available on request.

Acknowledgements

The authors gratefully acknowledge the funding by Italian Ministry of Education, University and Research (PRIN Grant n. 2020YKY7W4, ENRICH Project).

References

[1] FEMA 412. *Seismic restraints for mechanical equipment*. Federal Emergency Menagement Agency: 2002.
[2] FEMA E-74. Reducing the risks of nonstructural earthquake damage – A practical guide. Federal Emergency Menagement Agency, 2012.
[3] NTC-2018. *Aggiornamento delle «Norme tecniche per le costruzioni»*. D.M. 17 Gennaio 2018, Italy: 2018.
[4] Perrone D, Calvi PM, Nascimbene R, Fischer EC, Magliulo G. Seismic performance of non-structural elements during the 2016 Central Italy earthquake. Bull Earthq Eng 2016;2018:1–23. https://doi.org/10.1007/s10518-018-0361-5.
[5] Dhakal RP. Damage to non-structural components and contents in 2010 Darfield earthquake. Bull N Z Soc Earthq Eng 2010;43(4):404–11.
[6] Miranda E, Mosqueda G, Retamales R, Pekcan G. Performance of Nonstructural Components during the 27 February 2010 Chile Earthquake. Earthq Spectra 2012; 28(S1):453–71. https://doi.org/10.1193/1.4000032.
[7] Ricci P, De Luca F, Verderame GM. 6th April 2009 L'Aquila earthquake, Italy: Reinforced concrete building performance. Bull Earthq Eng 2011;9(1):285–305.
[8] O'Reilly GJ, Perrone D, Fox M, Monteiro R, Filiatrault A. Seismic assessment and loss estimation of existing school buildings in Italy. Eng Struct 2018;168:142–62.
[9] Vukobratović V, Fajfar P. Code-oriented floor acceleration spectra for building structures. Bull Earthq Eng 2017;15(7):3013–26.
[10] Merino RJ, Perrone D, Filiatrault A. Consistent floor response spectra for performance-based seismic design of nonstructural elements. Earthq Eng Struct Dyn 2020;49(3):261–84. https://doi.org/10.1002/eqe.3236.
[11] Lizundia B. Proposed Nonstructural Seismic Design Force Equations. Squaw Creek, California: SEAOC Convention proceedings; 2019.
[12] Rafiee R, Sharifi P. Stochastic failure analysis of composite pipes subjected to random excitation. Constr Build Mater 2019;224:950–61. https://doi.org/10.1016/j.conbuildmat.2019.07.107.
[13] Rafiee R, Habibagahi MR. Evaluating mechanical performance of GFRP pipes subjected to transverse loading. Thin-Walled Struct 2018;131(March):347–59. https://doi.org/10.1016/j.tws.2018.06.037.
[14] Rafiee R, Habibagahi MR. On The Stiffness Prediction of GFRP Pipes Subjected to Transverse Loading. KSCE J Civ Eng 2018;22(11):4564–72. https://doi.org/10.1007/s12205-018-2003-5.
[15] Soroushian S, Zaghi AE, Maragakis E", Echevarria A, Tian Y, Filiatrault A. Seismic Fragility Study of Fire Sprinkler Piping Systems with Grooved Fit Joints. J Struct Eng 2015;141(6).
[16] Tadinada SK, Gupta A. Structural fragility of T-joint connections in large-scale piping systems using equivalent elastic time-history simulations. Struct Saf 2017; 65:49–59. https://doi.org/10.1016/j.strusafe.2016.12.003.
[17] Merino RJ, Perrone D, Filiatrault A. Appraisal of seismic design methodologies for suspended non-structural elements in Europe. Bull Earthquake Eng 2022;20(15): 8061–98.
[18] Blasi G, Perrone D, Aiello MA, Pecce MR. Seismic performance assessment of piping systems in bare and infilled RC buildings. Soil Dyn Earthq Eng 2021:149. https://doi.org/10.1016/j.soildyn.2021.106897.
[19] Schneider SP. Flexural capacity of pressurized steel pipies. J Struct Eng 1998;124 (3):330–40.
[20] Ju BS, Gupta A. Seismic fragility of threaded Tee-joint connections in piping systems. Int J Press Vessel Pip 2015;132–133:106–18. https://doi.org/10.1016/j.ijpvp.2015.06.001.
[21] Tian Y, Filiatrault A, Mosqueda G. *Experimental Seismic Study of Pressurized Fire Sprinkler Piping Subsystems*. Technical Report MCEER-13-0001: 2013.
[22] Tian Y, Filiatrault A, Mosqueda G. Seismic response of pressurized fire sprinkler piping systems II: Numerical study. J Earthq Eng 2015;19(4):674–99. https://doi.org/10.1080/13632469.2014.994148.
[23] Blasi G, Aiello MA, Maddaloni G, Pecce MR. Seismic response evaluation of medical gas and fire-protection pipelines' Tee-Joints. Eng Struct 2018;173: 1039–53.
[24] McKenna F, Fenves GL, Scott MH, Jeremir B. Open system for earthquake engineering simulation. OpenSEES: University of Berkeley; 2000.
[25] EN 12845. Fixed firefighting systems - Automatic sprinkler systems - Design, installation and maintenance. European Standard: 2004.
[26] EN ISO 7396-1. *Medical gas pipeline systems - Part 1: Pipeline systems for compressed medical gases and vacuum*. International Organization for Standardization: 2007.
[27] ASCE/SEI 7-10. *Minimum Design Loads for Buildings and Other Structures*. American Society of Civil Engineers: 2010.
[28] NZS 4219. *Seismic performance of engineering systems in buildings*. New Zealand: 2009.
[29] NFPA 13. *Standard for the Installation of Sprinkler Systems*. National Fire Protection Association: 2007.
[30] Strutt JW. The theory of sound. London (UK): Macmillan and co.; 1877.
[31] Lowes LN, Mitra N, Altoontash A. A Beam-Column Joint Model for Simulating the Earthquake Response of Reinforced Concrete Frames. Berkeley: University of California; 2003.
[32] Soroushian S, Zaghi AE, Maragakis E, Echevarria A, Tian Y, Filiatrault A. Analytical seismic fragility analyses of fire sprinkler piping systems with threaded joints. Earthq Spectra 2015;31(2):1125–55. https://doi.org/10.1193/083112EQS277M.
[33] EN 10242. *Threaded pipe fittings in malleable cast iron*. European Standard: 1995.
[34] Blasi G. *Prove cicliche su giunti a T in rame - ReLUIS-DPC 2019-2021*. 2019.
[35] Perrone D, Filiatrault A, Peloso S, Brunesi E, Beiter C, Piccinin R. Experimental seismic response evaluation of suspended piping restraint installations. Bull Earthq Eng 2020;18(0123456789):1499–524. https://doi.org/10.1007/s10518-019-00755-5.
[36] Ambraseys NN, Smit P, Douglas J, Margaris B, Sigbjörnsson R, Ólafsson S, *et al.* Internet site for European strong-motion data. *European Commission, Research-Directorate General, Environment and Climate Programme* 2002. http://www.isesd.hi.is/ESD_Local/frameset.htm.
[37] Iervolino I, Galasso C, Cosenza E. REXEL: Computer aided record selection for code-based seismic structural analysis. Bull Earthq Eng 2010;8(2):339–62.
[38] EN 1998-1. *Eurocode 8 - Design of structures for earthquake resistance - Part 1: General rules, seismic actions and rules for buildings*. European Standard: 2005.
[39] Vamvatsikos D, Cornell CA. Incremental Dynamic Analysis. Earthq Eng Struct Dyn 2001;31(3):491–514.